Chapter 12
Synthesis of Nanostructured Materials by Thermolysis

Bheeshma Pratap Singh, Ramaswamy Sandeep Perala, Manas Srivastava, and Raghumani Singh Ningthoujam

Abstract The thermolysis synthesis for the different nanomaterials such as metal, metal oxides, hollow nanostructures, bimetallic, metal organic frameworks, and carbon dots is provided. Controlled shape and size engineering of particles has been performed using appropriate polyols. The polyols such as ethylene glycol (EG), polyethylene glycol (PEG), and glycerol are frequently used for the nanomaterial processing. The microwave assisted synthesis gives advantages such as fast heating, quick reaction rate, high yields of the product, and less reaction time as compared to the conventional heating techniques. Hydro/solvothermal routes are employed to obtain range of nanomaterials with controlled morphology and crystallinity compared to the other wet-chemical techniques. Sonochemical as well as ultrasonic spray pyrolysis approaches are also utilized for the synthesis of nanomaterials. Ultrasonication produces acoustic cavitation. The cavitation process leads to the formation of bubbles. During the collapse of bubbles, the tremendous amount of energy/high temperature and high pressures are liberated in very short time, and this can be used for synthesis of nanomaterials.

Keywords Nanomaterials · Polyol · Thermolysis · Microwave · Sonochemical · Hydrothermal · Solvothermal

Abbreviations

Nanoparticles	NPs
Microwave	MW
Ethylene glycol	EG
Polyethylne glycol	PEG

B. P. Singh (✉) · R. S. Perala · M. Srivastava · R. S. Ningthoujam (✉)
Chemistry Division, Bhabha Atomic Research Centre, Mumbai 400085, India
e-mail: bheeshmapratap@gmail.com

R. S. Ningthoujam
e-mail: rsn@barc.gov.in

R. S. Ningthoujam
Homi Bhabha National Institute, Mumbai 400094, India

A. K. Tyagi and R. S. Ningthoujam (eds.), *Handbook on Synthesis Strategies for Advanced Materials*, Indian Institute of Metals Series,
https://doi.org/10.1007/978-981-16-1807-9_12

Diethylene glycol	DEG
Tri-ethylene glycol	TEG
Butanediol	BD
Glycerol	GLY
Benzenehexa chloride	Bhc
Tri-ethanol-amine	TEA
Cetyl trimethyl ammonium bromide	CTAB
Sodium dodecyl sulfate	SDS
Polyethylenimine	PEI
Metal Organic Framework	MOF
Hollow Carbon Sphere	HCS

12.1 Introduction

Nanomaterials are regarded as backbone of nanotechnology and have shown promising applications in materials science, bio-physics, chemistry, biotechnology, etc. Synthesis plays a vital role in obtaining desired nanostructured materials. Moreover, synthesis of the nanomaterials with the environment friendly route, use of less toxic and less explosive reactants, and less reaction processing time is highly required. Precise control of shape and size of the nanoparticles (NPs) is necessary in order to tailor electrical, optical, magnetic, and catalytic properties. Nanostructured materials synthesized via thermolysis can provide the various shape and size of the particles which exhibit the different properties as compared to their bulk counterparts, and thus, they are useful in many applications such as optoelectronic devices, photocatalytic activity, data storage, bio-imaging, drug delivery, magnetic resonance imaging (MRI), fuel cell, photovoltaics, photodetector, super capacitors and hyperthermia, etc. [1–6].

Synthesis protocols play the pivotal role in controlling the morphology of the NPs, which finally determines their properties. Herein, thermolysis approach is presented for the synthesis of nanomaterials and their different applications. Thermolysis is a process of synthesis of compounds above room temperature but below the boiling points of the solvents. Generally, solvents used into thermolysis routes should have high boiling point. It may also include the process such as thermal decomposition, substitution, and addition of the ions or elements but we consider the case for thermolysis only when there is an involvement of heating in the presence of a solvent. The scope of thermolysis is very vast, and this can be also used in the preparation of organic and inorganic compounds. However, in this chapter, synthesis of inorganic materials such as metals, alloys, oxides, metal organic frameworks, etc., will be presented. Figure 12.1 represents the schematic of various routes of thermolysis, namely polyol, hydro/solvothermal, microwave (MW), sonochemical, and their applications.

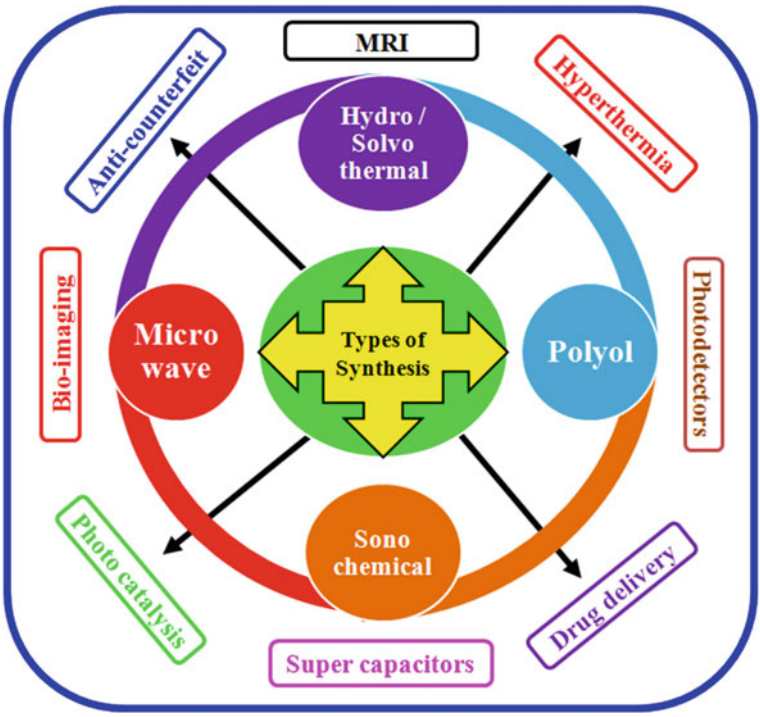

Fig. 12.1 Schematic representations depicting the various routes of thermolysis for synthesis of nanoparticles and their applications

12.1.1 Types of Solvents

On the basis of polarity, solvents can be categorized into two types—polar and non-polar solvents. Generally, polar solvents can dissolve polar molecule, whereas non-polar solvents can dissolve non-polar molecule. There are solvent molecules such as dimethyl sulfoxide (an organosulfur compound with the formula $(CH_3)_2SO$), N,N-dimethylformamide, which can dissolve polar or non-polar molecules. In addition, there are solvent molecules such as surfactant (oleic acid), which can dissolve polar molecule (water) and non-polar molecule (hexane, oil) simultaneously. Here, water-oil is immiscible, but miscible in the presence of oleic acid.

12.1.2 Polar or Hydrophilic Solvents

The solvent molecule having polarity due to presence of a functional group such as OH, which can mix with water molecule easily is considered as polar or hydrophilic solvent. The general structure of the solvents can be expressed as R-OH. Generally, this solvent has high boiling point; and in general, its boiling point increases with increase of OH contents in a molecule. The polar solvents with their structural formula and corresponding boiling points are represented in Table 12.1 [7].

12.1.3 Non-polar or Hydrophobic Solvents

Solvent molecule of non-polar character does not have static charges such as positive and negative charge separation, and in general, it is immiscible with water, and these are considered as non-polar or hydrophobic solvents. In this type of solvents, homogenous distribution of charges results in small dielectric constant. Moreover, non-polar solvents can dissolve non-polar substances such as oils, fats, and grease. Examples of non-polar solvents are summarized in Table 12.2 [8].

Using the hydrophilic solvents during the thermolysis process, agglomerated particles/compounds are prepared. Moreover, suitable use of capping agents such as sodium dodecyl sulfate (SDS), poly vinyl alcohol (PVA) which can exhibit less agglomeration, and nearly, monodispersed type compounds are prepared [9]. Moreover, in hydrophobic type solvents, octadecene, diethylether, and silicon oil have been used. By using these solvents and hydrophobic surfactant such as oleic

Table 12.1 Polar solvents and their corresponding boiling points

Solvents (Polar)	Chemical formula	Boiling point (°C)
Ethylene glycol (EG)	$HO–C_2H_4–OH$	197
Diethyleneglycol (DEG)	$HO–C_2H_4–O–C_2H_4–OH$	244
Tri-ethyleneglycol (TrEG)	$HO–(C_2H_4–O)_2–C_2H_4–OH$	291
Tetraethyleneglycol (TEG)	$HO–(C_2H_4–O)_3–C_2H_4OH$	314
Polyethyleneglycol (PEG)	$HO–(C_2H_4–O)_n–C_2H_4OH$	350
Glycerol (GLY)	$C_3H_8O_3$	290
Butanediol (BD)	$C_4H_{10}O_2$	235
Pentanediol (PD)	$C_5H_{12}O_2$	242
Methanol	$CH_3–OH$	64.6
Ethanol	$CH_3CH_2–OH$	78.5
n-Propanol	$C_3H_7–OH$	97
Acetic acid	$CH_3CO–OH$	117.9
n-Butanol	$C_4H_9–OH$	118
Water	H–OH	100

Table 12.2 Non-polar solvents and their corresponding boiling points

Solvents (Non-polar)	Chemical formula	Boiling point (°C)
Hexane	$CH_3(CH_2)_4CH_3$	69
Benzene	C_6H_6	80.1
Diethyl ether	$CH_3CH_2OCH_2CH_3$	118
Carbon tetrachloride	CCl_4	76.8
Diphenyl ether	$C_6H_5–O–C_6H_5$	257
Octadecene	$CH_3C_{15}H_{30}CH = CH_2$	315
Toluene	$C_6H_5CH_3$	111

acid, nearly monodispersed nanoparticles are prepared. Using polar solvents during the compound preparation, the thermolysis process can be categorized as (a) polyol, (b) hydrothermal and/or solvothermal, (c) microwave (MW) assisted synthesis, and (d) sonochemical synthesis.

12.2 Polyol Synthesis Route

Metal nanoparticles of Ag, Au, Pd, and Ni can be prepared by polyol route. Here, EG, PEG, and GLY solvents are used as reaction medium as well as reducing reagent. It restricts an extra addition of reducing agent. The presence of OH group in solvent helps in reducing metal ions. The polyol synthesis exhibits a range of features as compared to traditional sol–gel route such as it comprises high boiling points solvents, reducing properties for the metal synthesis, high solubility of metal salts comparable to water, and vast operating temperature choice. It also favors the synchronizing behavior toward surface functionalization, colloids of highly stable NPs, and vast range of flexibility of polyols ranging from low molecular weight EG to high molecular weight PEGs. Furthermore, it is easier to detach the polyols from the surface of NPs after synthesis by repeated washing with water, and thus, particles can be prepared at large scale. This route has been regarded as green, bio-compatible, and viable solvents, which is also extremely applicable for large-scale commercial synthesis of NPs [7].

12.2.1 Metal NPs

The solution processed polyol mediated synthesis has been emerged as the most effective successful route to prepare the metallic NPs with less agglomeration. Zero valent noble metals Au, Ag, Pd, Cu, and high electropositive Co and Ni metals are prepared. Also, this approach is further extended for the metals and its alloys comprised of particles with very less agglomeration, precise control over

morphology, and narrow size arrangement [10]. The precise control over shape and size shows tunability of opto-electronic, magnetic, catalytic, data storage capacities, etc. Xia and co-workers have synthesized the single crystal of Ag NPs via polyol mediated synthesis route. SilverNPs are prepared via reduction of silver nitrate salt precursor in the presence of ethylene glycol at higher temperature at the manifestation of polyvinyl pyrrolidone (PVP). Here, ethylene glycol acts as reaction medium as well as reducing agent while PVP as a capping agent. It was observed that addition of NaCl into the solution mixture increases the etching and oxidation of the twinned particles promoting the formation of monodispersed single crystal of Ag NPs [11]. In recent years, Pt NPs are extensively studied for their catalytic properties [12]. Yang and his co-workers reported the monodispersed Pt NPs are prepared via polyol route. It is reported that by mixing of $AgNO_3$ to the polyol, the morphology of Pt NPs changes. Here, nitrate anion significantly reduces the degree of reduction of Pt(II) and Pt(IV) via ethylene glycol. Generally, PVP is used as regulating and stabilizing agent for the selective growth of nanocrystal in well-defined shape. It is reported that monodispersed Pt nanocrystals with different shapes comprising of cubes, cuboctahedra, and octahedral can be prepared by polyol method. In the synthesis process, $AgNO_3$ solution containing Ag ion shows a vital part for the controlled morphology of Pt NPs [13]. Xia and his co-workers reported the uniform cuboctahedral PdNPs can be prepared by using simple polyol synthesis route. In the typical synthesis of Pd NPs, $Na_2[PdCl_4]$ metal precursor is mixed thoroughly into EG heated at 100 °C in the presence of PVP [14]. The reaction mixture is largely established by cuboctahedra composed with twinned particles. The chloride as well as O_2 anions are accountable for the oxidative etching of twinned NPs. The twinned NPs are stable under Ar atmosphere. Moreover, these twinned NPs are vanished by revealing the sample to air. Thus, twinned NPs are more sensitive due to the higher concentration of surface defects as compared to cuboctahedra. This demonstrates the occurrence of an oxidant in reaction medium affording a way to control the formation of well-defined morphology of PdNPs. Monodispersed gold nanoboxes with highly truncated cubic shape have been synthesised employing silver nanocubes as a sacrificial template in which silver nanocubes react with an aqueous $HAuCl_4$ solution by following reaction process:

$$3Ag\ (s) + HAuCl_4(aq) \rightarrow \cdots Au(s) + 3AgCl(aq) + HCl(aq)$$

These polyols mediated silver and gold NPs treasure their applications in diverse zones of claims in photonics, catalysis, and surface enhanced Raman spectroscopy (SERS)-based sensing [15]. For the comparatively less-noble metals, the reducing capacity of the polyol reaches to its higher limit at elevated temperature (>230 °C). Even though if reduction process continues to happen, quick thermal decomposition of the polyol obstructs the nucleation of NPs and impedes their separation subsequent to synthesis. Moreover, by lowering the temperature, less-noble metals such as Co^0 and Ni^0 can be deoxidized by the polyol. At elevated temperature (>150 °C) reducing ability of polyol favors the reduction of these metallic ions to their

zero-valence metal from Co^{2+}/Ni^{2+} to Co^{0}/Ni^{0}. Meanwhile at the lower temperature (<150 °C), the bonding of ions and molecules to metal ion stability of the polyols as well as the existence of OH-groups entails the re-oxidation to Co^{2+}/Ni^{2+} [16].

12.2.2 Metal Alloys

The bimetallic NPs show the better data storage capacity as compared to monometallic counterparts. In the synthesis of FePt metal alloys, platinum and iron acetyl-acetonates reduce in the presence of ethylene glycol. It has been suggested that in presence of 1,2-hexadecanediol as the reducing reagent, great quality FePt NPs are obtained via the reduction of $C_{10}H_{16}FeO_4$ and $C_{10}H_{16}O_4Pt$. The monodispersed FePt NPs having *fcc* phase show disordered structure. Upon annealing the sample at 650 °C under inert argon atmosphere, structural phase change occurs via disordered *fcc* to ordered L10 phase. The elemental configuration is precisely tuned via tailoring the comparative amounts of metal precursors of Fe (II) and Pt(II) [17]. Also for the preparation of monodispersed FePd NPs, altered polyol mediated synthesis has been implemented. Paladium acetyl acetonate Pd $(acac)_2$ is effortlessly dissolved in diphenyl ether. The 1,2-hexadecanediol is used as a reducing agent, while oleic acid and oleylamine is used as stabilizer. The solution mixture is heated below the boiling point of diphenyl ether and refluxed [18]. The as-prepared FePdNPs are annealed for its structural ordering from disordered *fcc* phase to L10 ordered phase in vacuum [18, 19]. Fievet et al. have also reported the synthesis of various other metal alloys such as $Ni_{1-x}Co_x$, FeNi, Co_xCu_{1-x}, and FeCoNi [20]. Metal carbides such as Co_3C, Co_2C, Ni_3C have been prepared and they exhibit high coercivity in magnetic study. These carbides-based alloys have shown promising applications in data storage [7].

12.2.3 Metal Oxides

This synthesis protocol is effectively extended to synthesize the metal oxides NPs. Highly water-dispersible Fe_3O_4NPs are prepared via thermal decomposition of iron acetylacetonate in the presence of PEG comprising PVP and polyethylenimine (PEI). Fe_3O_4 NPs layered with PEG/PVP and/or PEG/PEI displayed an excellent dispersion constancy in water. The surface of prepared Fe_3O_4NPs can be modified by the use of suitable polymer additives [21]. Monodispersed magnetite Fe_3O_4NPs are prepared using tri-ethylene glycol (TEG). TEG reduces $Fe(acac)_3$, and finally, magnetite is obtained [22]. Polyol mediated submicron-size monodispersed ZnO NPs are prepared via hydrolysis of zinc acetate dehydrate and diethylene glycol [23]. Feldman and Jungk have reported the highly crystalline monodispersed Cu_2O, TiO_2 and Nb_2O_5NPs via polyol technique. Also Y_2O_3, Cr_2O_3, $ZnCo_2O_4$, ZnO:In^{3+}, CeO_2, Mn_2O_4 NPs have been successfully synthesized for their different aspect of

applications [24]. Very vast ranges of oxide nano-materials have been prepared via polyol for their various applications. Oxides such as MnO_2, Mn_3O_4, Cu_2O, $NiCo_2O_4$ are used as catalysts, while photocatalytic properties have been reported for ZnO, Cu_2O and $BiVO_4$ [7]. Also magnetic oxides NPs such as Fe_2O_3, Fe_3O_4, Gd_2O_3, and spinel ferrites such as $MgFe_2O_4$, $CoFe_2O_4$, $ZnFe_2O_4$ are reported for their biomedical applications. Dye sensitized photovoltaic cells for broad band-gap diluted semiconductors, namely ZnO, TiO_2 have reported. Also high-power batteries applications of the oxides such as V_2O_5, MnO, Mn_2O_3, SnO_2, $CoMn_2O_4$, $LiFePO_4$, and $LiMnPO_4$ have been reported [25, 26]. The involvements of hydrolysis and reduction reactions are major chemical reactions during the polyol synthesis. The micron-size metal particles with tailored morphology are attained in the deficiency of water, while water entails the reduction and increases the hydrolysis which thus results information of metal oxides through polymerization. Poul et al. have reported the layered hydroxide acetate structures of zinc, cobalt, and nickel metals. Presence of high degree of water contents favors the hydrolysis and condensation reaction for layered geometry formation. The use of acetate precursors as compared to its chlorides and sulfates counterparts promotes to the precipitation of metal, oxides, and hydroxides. The precipitation process majorly depends upon hydrolysis ratio (water to metal molar ratio is termed as hydrolysis ratio) [27]. Furthermore, Prevot et al. have extended the polyol synthesis route for the synthesis of layered double hydroxides $[Ni_2Al(OH)_6]Ac{\cdot}nH_2O$, and $[Co_2Al(OH)_6]Ac{\cdot}nH_2O$ using acetate precursors in polyol [28]. Molybdates and tungstates AMO_4 (A = Ca, Ba, Sr, Mg, M = Mo, W) derivative compounds are successfully synthesized via polyol mediated route at ambient temperature. $CaWO_4$ and $CaMoO_4$ show the intrinsic photoluminescence without any impurity ions doping in its bluish green region (400–540 nm). After incorporating the Eu^{3+} and Sm^{3+} ions in these host matrices, sharp characteristics f-f transitions of these activators (Eu^{3+} and Sm^{3+}) exhibit red color emission. MoO_4^{2-} and WO_4^{2-} act as efficient emission centers which absorbs the UV light and transfer to the corresponding activator ions, and strong emission in red region is observed due to energy transfer from MoO_4^{2-} and WO_4^{2-} to Eu^{3+} and Sm^{3+} [29–32]. Highly crystalline and luminescent phosphates and fluorides-based compound are obtained [33, 34].

Moreover, the polyol mediated synthesis technique is extensively employed for synthesizing nanostructured chalcogenides. In chalcogenides system, more often sulfide-based compounds are discussed. Usually, CH_4N_2S, hydrogen sulfide, or soluble metal sulfides such as Na_2S are utilized as precursors for the source of sulfur. The polyol mediated synthesized metal chalcogenides have been activated in contemporary years for its explicit assets and applications in vast domain. The $CuInSe_2$ and Cu_2ZnSnS_4 are used in photovoltaic, while In_2S_3 and SnS are used in photo-detectors. Also, $ZnIn_2S_4$, Bi_2Te_3, and Sb_2S_3 are used as photocatalysts, thermo-electrics, and in lithium-ion batteries, respectively [7].

12.2.4 Core@Shell Nanomaterials

In polyol mediated synthesis of core-shell nanoparticles such as ferrimagnetic $CoFe_2O_4$ as a core and antiferromagnetic CoO as shell with high degree of crystallinity, giant exchange bias effect is observed. This exchange bias coupling is impressively employed in memory and switching devices [35]. Two-step polyol mediated synthesis under N_2 gas bubbling is reported for core@shell Cu@Ag NPs. Since oxidation of copper takes place in the existence of oxygen in the solution, hence N_2 gas is passed to suppress the oxidation of copper via core@shell formation. Reduction of Ag^+ is faster as compared to copper oxidation and its reduction to Ag^0 leads suppression of nucleation and growth of Ag NPs [36]. Nguyen et al. have reported the star shaped $Fe_{3-x}O_4$–Au core@shell structured nanomaterials using polyol synthesis. Fe_3O_4 core comprised with gold shell has been prepared via polyol method in which hydroquinone is used as reducing agent. The prepared core@shell materials are utilized for the chemical sensors [37]. The bi-functional behavior of highly luminescent core@shell $CaMoO_4$:Eu@$CaMoO_4$ and its hybrid formation with Fe_3O_4 for its hyperthermia and bio-imaging applications has been reported [38]. Highly luminescent β-$NaY_{0.8}Eu_{0.2}F_4$@γ-Fe_2O_3 core-satellites NPs are prepared for its dual mode magnetic resonance as well as bio-imaging applications [39].

12.2.5 Carbon Dots

Recently, carbon dots have attracted a noticeable attention owing to their superior high quantum yield, less toxicity, and high chemical stability. These properties may be very useful in bio-imaging and optoelectronics application. Carbon dots may be utilized in bio-imaging. Also, narrow emission band of red color with blue and green component covers its utility in full color display. Feldman and his co-workers reported the preparation of ultra-small carbon dots ∼3–5 nm via straightforward and effective polyol route. The presence of $MgCl_2 \cdot 6H_2O$ salts promotes the nucleation of the carbon dots via thermal decomposition of glycerol, diethylene glycol, and PEG 400. Further modification of prepared carbon dots with $TbCl_3$/$EuCl_3$, an efficient Förster resonance energy transfer takes place via the carbon dots to the lanthanide ions resulting the sharp characteristics emission of terbium ions (green) and europium ions (red) with a very high quantum yields ∼85%. The synthesis strategy and full color display for as-prepared carbon dots and modified with Mg^{2+}, Tb^{3+}, and Eu^{3+} have been presented in Fig. 12.2. The highly efficient multicolored C-dots prepared via polyol route can be very noteworthy for molecular imaging and optoelectronics [40].

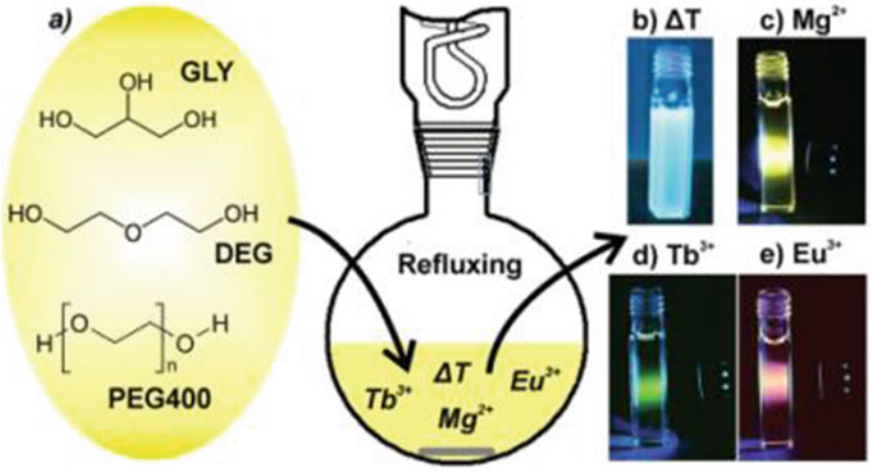

Fig. 12.2 Polyol-assisted synthesis of C-dots: **a** Protocol used for the synthesis; **b** T/PEG (λexc = 366 nm) exhibits blue color emission; **c** Mg^{2+}/PEG; gives yellow color emission; **d** Tb^{3+}/PEG; provides green color emission and **e** Eu^{3+}/PEG; reveals red color emission under blue-LED excitation λ_{max} = 465 nm). Reproduced with permission from RSC publisher [40]

12.3 Microwave Synthesis (MW) Route

Microwave (MW) synthesis approach is an emerging green chemistry route under which materials can be prepared to an atomic level. MW route offers to prepare the multifunctional nanomaterials which establish their profound applications in area of energy production, nano-biomedicine, nano-electronics, etc. In this approach, the choice of green solvents as well as energy efficiency is major parameters to control the NPs growth. Also, MW heating is reflected as a more competent mode to regulate the heating during reaction process since it requires less energy consumption as compared to traditional routes. Furthermore, use of ionic liquids with solvent free as well as nontoxic precursors approach promotes the lucrative green synthesis of NPs. The synthesis process for the nanomaterials has been dependent on innumerable factors, namely temperature, pressure, solvents, synthesis time, etc. Shape and sizes of particles are precisely controlled by MW irradiation [41]. The microwave radiation refers to a part of an electromagnetic spectrum which has radiation frequencies vary between 300 MHz and 300 GHz. The MW approach accelerates the reactions because polar solvent molecules absorb MW energy and thus produce tremendous extent of thermal energy via disturbing the alignment of the molecules with respect to the external field.

In the MW-assisted synthesis, heat up of the reaction mixture is considerably quicker at ambient pressure as compared to convection-based orthodox heating process. The chemical reactions, which are not feasible under the conventional heating, can be executed under like conditions with the MW heating. The experimental findings could not be well explained by the consequence of MW heating only, promoting the clarification of the continuation of the non-thermal MW properties [42].

12.3.1 Principle Behind MW Heating

The MW heating includes two-fold key mechanisms, namely dipolar polarization as well as ionic conduction. Generally, MW can produce heat to material with polar molecules and through ionic conduction. During the MW heating, polar solvents like water molecules attempt to orient with the fast changing alternating electric field which leads to heat generation by the process of rotation, friction, and collision. This type of heat generation leads to dipolar polarization. Moreover, ionic movement into the solution will be dependent on the alignment of the electric field. The constant movement of ions into solution with changing directions leads to rise in local temperature via friction and collision (Fig. 12.3b) [43]. In case of conducting and semiconducting, nano-material heat generation takes place by formation of electric current with involvement of electrons and ions. Energy dissipation in these systems is mainly because of resistance of the material, and this process is governed via ionic conduction namely.

12.3.2 Conventional Versus MW Heating Process

Electric furnace and/or oil bath are frequently used in the traditional heating. Firstly, reactor chambers are heated followed by subsequent heating of reactants via heat convection and/or conduction mechanism. Reactor plays a mediator role, and it transfers the thermal energy via outside heat resource to the solvent and finally on the way to reactants. Sample core proceeds much higher time duration to reach the set temperature value which causes inefficient and inhomogeneous reactions (Fig. 12.3a). It may thus not much effective in mass production. Moreover, in MW heating only target materials heating takes place and homogenous heating can be done. In this type of heating, entire heating of furnace and oil bath does not takes place, and thus, it saves time and energy [41].

12.3.3 MW Effect on Rate of Reaction

Specific reactant energy (E_R) is required to initiate any molecular reaction between A and B. For the proceedings of the reaction, the reactants must attain the activation energy to acquire transition state (TS). Thus, activation energy is indicated by E_{TS}-E_R, and this much energy is engaged by the reactants from the reaction surroundings. Finally, formation of products with lower energy E_P is obtained. Use of MW irradiation does not modify the activation energy. It offers an excessive impetus to complete the reaction more rapidly as compared to conventional heating. Since the MW transfers the energy to the molecule in10^{-9}s while the molecular relaxation takes time in a period of 10^{-5}s, rapid MW energy transfer as compared to

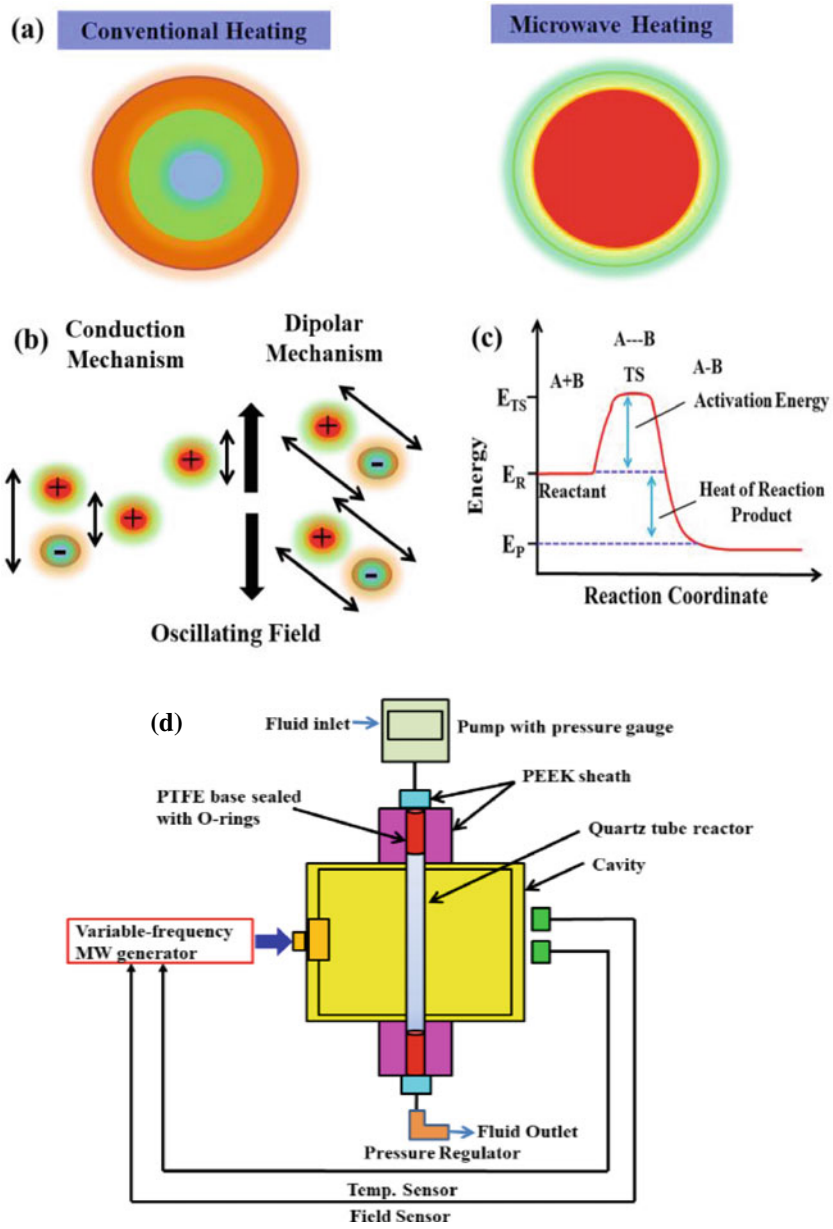

Fig. 12.3 **a** Conventional and MW heating, **b** dipolar and ionic conduction mechanism, **c** effect of MW on reaction medium, and **d** MW reactor for synthesis of nanomaterials. This is redrawn from references [41–44]

molecular relaxation leads to higher instantaneous temperature within the reaction medium which finally speeds up the reaction rate (Fig. 12.3c) [42].

The un-interrupted flow-type reactor with appropriate pressure allows uniform heating of the reaction. This reactor is required during this synthesis for its fast and mass production synthesis of nanomaterials. The constant flow from MW reactor is outfitted to a high-pressure connection. A uniform electromagnetic field alongside a tube-shaped reactor is produced at the midpoint of a cylindrical MW cavity (Fig. 12.3d). The applied MW reactor system comprised of a MW generator has operating frequency and power 2.5 GHz ± 200 MHz and 100 W. The reactor system automatically records the change in resonance frequency shift. A radiation thermometer is employed for the temperature measurement of the reaction solution via slit of cavity. The pressure to the reaction mixture is maintained via a pump and guided toward the quartz reactor tube. The pressure regulator is applied to vary the pressure required. The quartz reactor tube is linked with the sheath that provides the necessary pressure to sustain ∼10 MPa and finally closed through a Kalrez O-ring [44].

The role of solvent during synthesis shows a vital part in the synthesis of nanomaterials for the green approach synthesis. Generally, MW heating ability infers the capability of a solvent to change the MW energy into thermal energy at a specified MW temperature and frequency. The heating ability has been generally governed by dielectric loss tangent(tan $\delta = \varepsilon''/\varepsilon'$) where ε' and ε'' are dielectric constants (see in Table 12.3) [45].

The loss tangent mainly relies on the temperature and MW frequency. The penetration depth profile is strongly dependent on temperature and frequency. The

Table 12.3 Solvents and their corresponding loss tangent at 20 °C

Solvents	tan δ
Ethylene glycol	1.349
Ethanol	0.939
2-propanol	0.800
Methanol	0.660
1,2-dichlorobenzene	0.279
N-methyl-2-pyrrolidone	0.280
1-butyl-3-methylimidazolium hexafluorophosphate	0.190
Acetic acid	0.172
N,N-dimethyl-formamide	0.159
1,2-dichloroethane	0.130
Water	0.119
Chlorobenzene	0.990
Acetone	0.053
Tetrahydrofuran	0.046
Dichloromethane	0.042
Toluene	0.04
Hexane	0.02

penetration depth states to the point at which nanomaterials preserves 37% of the primary irradiation source power. The penetration depth decreases as loss tangent increases. The solvents with low loss tangent show high penetration depth, while high loss tangent possess small penetration depth. The MW penetration depth profile through a solvent is given as

$$D_p = \left(\frac{\lambda_o}{2\pi}\right)\left(\frac{\sqrt{\varepsilon'}}{\varepsilon''}\right)$$

λ_o is the wavelength of the MW radiation, and its value is observed to be 0.122 m at 2.45 GHz. H_2O is frequently utilized solvent for the preparation of nanomaterials via MW. The penetration depth values at 22 °C for water solvent at 2.45 GHz are 1.8, cm while its value is 0.34 cm at 5.79 GHz MW treatment [41]. Tangent loss for the different solvents used in the MW-assisted route at 2.45 GHz is mentioned in Table 12.3 [46]. During the MW supported inorganic nanostructure materials, H_2O (tan δ = 0.119) and alcohols are widely utilized for their good MW heating. Polyol such as EG has loss tangent tan δ = 1.349 and high boiling point (∼197.9 °C) with strong reducing capability, allow fairly elevated temperatures for the synthesis of inorganic nanostructured materials. The dielectric behavior of solvents generally alters considerably with respect to temperature. Solvent such as ethanol exhibits decent MW absorbing property with loss tangent 0.94 at room temperature. Moreover, loss tangent decreases from 0.27 to 0.08 as temperature rises from ∼100 to 200 °C. Heating involved during MW synthesis using ethanol solvent is mainly due to the dipolar polarization phenomena. The MW absorbing property decreases as temperature increases. The rise in temperature decreases the viscosity and frictions among the molecules [47].

In case of ionic liquids such as 1-butyl-3-methylimidazolium hexafluorophosphate, heating takes mainly due to the ionic conduction phenomena. The MW absorbing property increases with rise in temperature in case of the ionic liquids [8].

12.3.4 Synthesis of Metal NPs

The metallic nanostructures with different morphologies, namely sphere, nanosheets, nanorods, nanowires, nanotubes, and dendrites have been quickly synthesized via MW heating. The morphology as well as dimension of metallic NPs might be precisely organized by varying the reaction mixture condition such as precursors concentration, proper selection of the solvent, surfactant, and reaction temperature [48]. Green MW approach is employed for the synthesis of noble metals, namely Au, Ag, Pd, and Pt, nano-particles using red wine and/or grape pomace extract which play the role of green solvent source, reducing as well as stabilizing reagent [49]. Reducing agent free MW-assisted Au NPs is prepared using $HAuCl_4$ in aqueous phase. Synthesized gold NPs show aggregation and uncontrolled growth

[50]. MW-assisted hydrothermal approach is applied for the folic acid targeted Au NPs using $HAuCl_4$ and NaOH. The folic acid targeted Au nanoparticles is used for detection of Hela Cells since tumor cells over express as the folate receptors to the cancer cells [51]. Rapid MW supported approach is reported for the synthesis of monodispersed Ag NPs. During the synthesis, basic amino acid like L-lysine or L-arginine is used as a reducing reagent while starch is used as a shielding agent. In a typical synthesis process, 0.4 mmol of soluble starch and 0.16 mmol of L-Lysine or L-arginine are added to 4.0 mL of deionized water followed by addition of 20 mmol aqueous solution of $AgNO_3$ and stirred. The temperature of reaction mixture is kept at 150 °C under MW irradiation. Monodispersed Ag NPs are obtained in a very short period of time ~10 s [52].

Colloidal Pt NPs are prepared by an aqueous solution comprising H_2PtCl_6 and 3-thiophenemalonic acid under MW irradiation (power ~300 W) for 8 min. duration. NPs size has been organized through adjusting the molar ratio of the reaction precursors [53]. Pt nanoclusters with a porous interconnected nanostructure are attained via MW heating to an aqueous solution containing K_2PtCl_4 and 2-[4-(2-hydroxyethyl)-1-piperazinyl]-ethane sulfonic acid for 12 s only. The Pd NPs have been prepared under MW heating in quick time 20 s only, using $PdCl_2$, glucose, and PEG as a capping agent in aqueous solution [54]. MW-assisted single crystal Cu nanowires at 120 °C for 2 h is prepared by using $CuCl_2$, hexadecylamine, ascorbic acid into water. Ascorbic acid as well as hexadecylamine play significant role in controlling morphology and aspect ratio of Cu nanowires [55]. MW approach is further extended for the preparation of luminescent silicon QDs. During synthesis of Si nano-wires, glutaric acid is used at 185 °C for 15 min. Highly luminescent, dispersible and photo as well as pH stable Si quantum dots show their potentiality for the relevance in cellular imaging [56].

12.3.5 Metal Oxides

Substantial work has been dedicated to MW-assisted synthesis of numerous metal oxides owing to its remarkable properties, extraordinary constancy as well as extensive applications in various arenas. MW-assisted syntheses of metal oxide nanomaterials involve a water-soluble metal salt as the metal source, an alkaline component and a surfactant to govern the morphology and dimension of the nanomaterials. MW-assisted synthesized metal oxides such as ZnO, SnO, SnO_2, TiO_2, Fe_3O_4, Co_3O_4, CuO, MnO_2, ZrO_2, WO_3, MoO_3, CeO_2, Nd_2O_3, and Y_2O_3 are reported [57–70]. Also metal tungstates such as AWO_4 (A = Ca, Sr, Ba, Fe, Co, Ni, Mn, Zn, Ag/In), gallate $ZnGa_2O_4$, spinel metal ferrites AFe_2O_4 (A = Mg, Zn, Ni, Mn, Co), metal aluminates MAl_2O_4(M = Zn, Co), perovskites $BiFeO_3$, $ATiO_3$(M = Ba, Sr, Pb), metal molybdates $AMoO_4$ (M = Ba, Ca), and metal vanadates MVO_4 (M = Bi, Ce, Y, La) are also explored [41].

Fe_3O_4 is a significant magnetic functional material and has been found its profound applications in diverse areas of research such as contrast agent in MRI,

hyperthermia, gene separation, drug delivery, etc. [71, 72] Under MW irradiation, Fe_3O_4 NPs have been generally prepared by means of Fe(III) salt and/or salts of Fe (III) and Fe(II) dissolved in the water and a reducing agent present in an aqueous phase [73]. Also, surfactant free Fe_3O_4 NPs are prepared using an oxidized iron foil such as Fe_2O_3 into deionized water. During synthesis, no additive like alkali, acid, or surfactant is used. Homemade MW oven at 700 W fixed operating powers for 30 min is applied during synthesis. The as-synthesized Fe_3O_4NPs exhibited magnetization of Ms $\sim$ 51.29 emu g^{-1} [74]. The MW-assisted approach for preparation of Fe_3O_4NPs is reported by using an aqueous solution containing $FeCl_3$, $FeSO_4$, and ammonia [73]. Also, iron oxide/oxyhydroxide NPs have been synthesized under MW irradiation. The well-ordered growth as well as assembly of NPs are commonly observed due to gentle reaction of the reactants (iron salt and sodium hydroxide) [75].

12.3.6 Metal Chalocogenides

Functional metal sulfides nanomaterials have shown their significant uses in optoelectronics and nanomedicines as a carrier drug, bio-imaging, etc. [76, 77]. MW approach assists the fast production of metal sulfide nanostructures and has triggered a great deal of interest owing to its small processing time. Generally, water-soluble metal precursors are used as sulfur source during MW-assisted sulfide synthesis in aqueous phase. Surfactant is used to control the precise size and morphology of particles. Nanostructured metal sulfides are prepared with different shapes and sizes of particles via MW-assisted approach in aqueous solution such as PbS, CuS, CdS, ZnS, Ag_2S, Bi_2S_3, HgS, $AgInS_2$, $AgIn_5S_8$, $CuInS_2$, and $CdIn_2S_4$ [78–88]. The most common sulfur sources used during the metal sulfide synthesis in aqueous solution comprised of Na_2S, CS_2, $Na_2S_2O_3$, NH_2CSNH_2, $NH_2NHCSNH_2$, CH_3CSNH_2, and 3-mercaptopropanoic acid [41]. The synthesis of metal telluride nanomaterials is still tricky related to its metal selenides counterparts. CdTe is an important class of semiconductor material which has wide application in solar cell and in infrared optical window. The p-n junction solar cell is formed via sandwiching CdTe with CdS. The conventional aqueous solution way to prepare the CdTe nanocrystals generally takes prolong time duration. During MW synthesis, NaHTe is normally used as the source of tellurium. High-quality nanocrystal of CdTe is reported via MW-assisted synthesis. An aqueous solutions consisting of $CdCl_2$, NaHTe, 3-mercaptopropionic acid, and NaOH are used. During synthesis, high yield of the product is simply attained by tuning the reaction time and temperature. This approach permits the fast synthesis of CdTe nanocrystals with wide spectral range covering from green to NIR at lower temperature ranges [89]. MW-assisted metal selenides nanostructured materials are less reported as compared to nanostructured metal oxides and sulfides. It is perhaps due to high cost metal precursors, a lesser amount of availability of selenide sources, and difficulties in the synthesis. The quickness of MW-assisted route is

more notable for metal selenides with considerably less reaction time period up to minutes. MW synthesis of CdSe, PbSe, and Cu_2Se NPs is reported by taking metal acetates and/or sulfide precursors under refluxing conditions with Na_2SeSO_3 into aqueous solution. Crystal structure of CdSe NPs is reliant on the reaction time duration under MW irradiation. CdSe nanocrystal exhibits cubic phase for MW heating of 10 min; while for prolong duration time of 30 min of MW irradiation, hexagonal CdSe nano-crystal is obtained [90].

12.3.7 Core@Shell Structure

As for as controlled size and shape of particles, synthesis of nanomaterials and tailoring their properties at nano-scale are concerned, and core-shell strategy has been employed by simple coating of organic and/or inorganic nanomaterials. Core@shell formation of the nanomaterials decreases the surface energy of the arrangement. Outer shell coated over inner core materials exhibit significant role to advance the reactivity and oxidation ability of the interior core manufacturing. Core@shell anomaly comprises inner inorganic core covered by outer shell forms the heterogeneous system [91]. Core@shell nanostructured materials are synthesized via MW-assisted route in aqueous solution. Au@Pd and Au@Pt structures are attained through the reduction of Au(III) complexes. The reduction of chloro-complexes of Au and nano-powders of Pd and Pt takes place under hydrothermal, and MW irradiation leads to the realization of bimetallic core@shell structure [92]. Also Se@C core@shell nanostructure is obtained using starch and H_2SeO_3into deionized water under MW-assisted hydrothermal process. The prepared product comprised of Se nano-rod as the core and amorphous carbon as the shell materials [93]. Pd@Pt core@shell nanostructures in aqueous solution are synthesized using K_2PtCl_4, $PdCl_2$, and CTAB under MW irradiation. Morphology of the core@shell nanostructures is precisely organized by changing the Pt and Pd molar ratio of precursors [94]. Rapid, modest, and one step MW supported approach to formulate the gold coated with silica shell NPs(Au@SiO_2) has been reported. This approach circumvents the time wasting orthodox routes (Fig. 12.4).

The MW-assisted scheme deals with the uniform SiO_2 coating over the colloidal AuNPs, exploiting silane as the coupling reagent. Monodispersed AuNPs (particle size $\sim$16 nm) are obtained by employing citrate reduction approach. The tetra-ethoxysilane TEOS is used during the silica coating as coupling reagent under the MW irradiations. Dynamic light scattering results the excellent dispersion of the prepared NPs in aqueous medium. Additionally, surface functionalization of silica-coated AuNPs (Au@SiO_2) is perfumed via conjugation of different functional assemblies as amine (–NH_2), carboxylic (–COO) and alkyl groups [95].

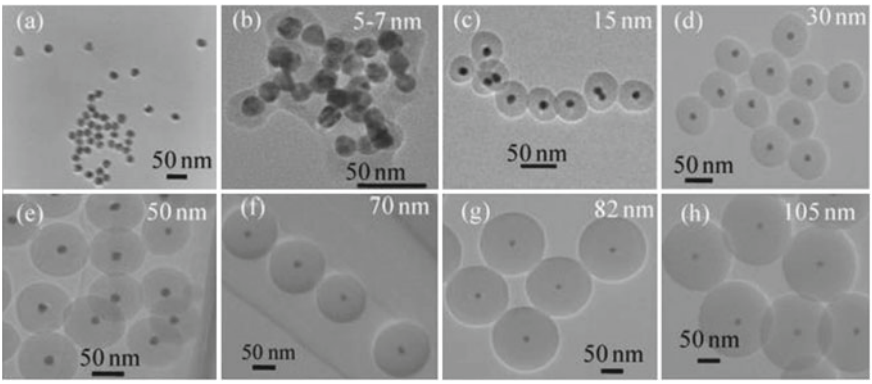

Fig. 12.4 TEM Micrographs of **a** Au NPs **b–h** Au@SiO_2NPs with various silica shell thicknesses with varying concentration of TEOS 1, 2, 3, 5, 10, 15, and 20 nm. Reproduced with permission from Elsevier publisher [95]

12.3.8 Hollow-Type Structure

In recent times, the hollow-archetype structures comprised of inorganic and/or organic composites have fascinated a lot of attention owing to their low density, enormous surface area, and induced large porosity in the sample surface. These assets of hollow structured materials could find their powerful applications in diverse research zones such as catalysis, super capacitors, sensors, drug delivery and microcapsule reactors, etc. [96–99]. The conventional heating-based engineering tactics are broadly introduced to synthesize the hollow-type designs of inorganic nano-materials. Moreover, these routes involve precious metal precursors and long duration reaction time. Thus, MW-assisted approach has been admitted for the synthesis such hollow-types design due to its remarkable highlights such as uniform volumetric heating, fast reaction rate, and energy consumption [100]. The hollow porous carbon sphere is synthesized via MW-assisted method and possesses the following such as amorphous phase of porous structure, uniform size, high pore volume, and highly dispersed, which are used as anode materials in lithium-ion batteries [101].

12.4 Hydro- and/or Solvothermal Approach

Hydro- and/or solvothermal process is a wet-chemical synthesis approach commonly implemented for preparing nanomaterials with precise particle size, shape, and composition. During the synthesis, high vapor pressure is generated by the consequence of heating of the reaction mixture in a sealed vessel above the ambient temperature and pressure. The discrete feature of hydro and/or solvothermal

Table 12.4 Characteristics of usually employed solvents during hydrothermal and/or solvothermal approaches [102]

Solvent	Formula	Critical temperature (°C)	Critical pressure (MPa)
Water	H_2O	374	22.09
Ethylenediamine	$H_2N–C_2H_4–NH_2$	319.88	62.09
Methanol	CH_3OH	239.19	8.09
Ethanol	C_2H_5OH	241.09	6.09
Toluene	C_7H_8	320.59	4.19
Ethanolamine	$HO–C_2H_4–NH_2$	398.24	8

treatment is the deployment of capping ligands to control the growth of the particles during synthesis and prevent the agglomeration of the nanomaterials in solutions. The chelating ligands associated with surface of particles can provide versatile functional groups for bio-conjugation. The limitation of the hydro- and/or solvothermal method suffers scalability of the product preparations as well as limiting operating temperature at 300 °C into a Teflon line autoclave (Table 12.4).

Nanomaterials production through hydrothermal/solvothermal approach in aqueous solution involves crystal nucleation followed by growth. The nanomaterials can be prepared into desired shape, size, and morphology of particles by tuning the reaction parameters such as temperature, pH, precursors concentrations, and surfactants as additives. The mechanism governing the controlled shape, size, and morphology of particles via varying the reaction conditions is large due to nucleation and growth rates which rely on supersaturation. The term supersaturation is distinct as the proportion of the real concentration to the saturated precursor concentration into the solution [103, 104].

When the solute precursor solubility exceeds its maximum value into the solution, resulting solution becomes supersaturated thus promoting the nucleation. The synthesis process is completely irreversible one in which precipitation of the solute leads to the nucleation of macroscopic size crystals [105]. After nucleation, the sequential growth of crystals takes place. The growth of crystals involves the integration of growth units. The growth units correspond to the similar crystal entities exhibiting the identical and/or dissimilar structure from the precursor solution resulting in an increase in sizes. The schematic representation of the involved mechanisms of crystal growth via hydrothermal/solvothermal methods has been shown in Fig. 12.5. Since plentiful availability, less toxicity, and an elevated dielectric constant are required, and water has been frequently utilized solvent in the hydrothermal/solvothermal routes. In this technique, the values of critical temperature and pressure of water are ∼374 °C and ∼22 MPa. The variation in temperature and pressure infers the changes in the property of water. This change is even more profound above its critical point value. At room temperature, the dielectric constant value for water is 78. The high value of dielectric constant promotes the dissolution of polar salts into it. In the critical zone, the dielectric constant of water decreases (∼10) via increase in temperature and decrease in

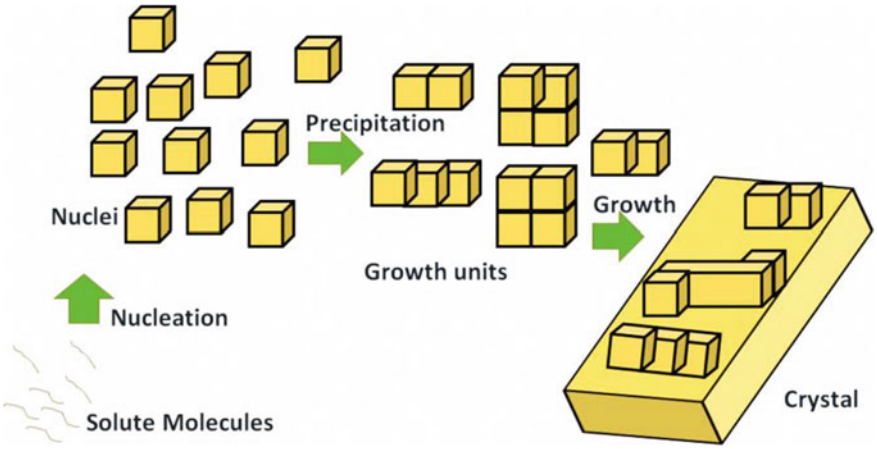

Fig. 12.5 Schematic representation of crystal growth mechanism for the hydro- and/or solvothermal processes. This is redrawn from references [103–106]

pressure. The dielectric constant value drops considerably in the range ~2 to 10 above its critical point [106]. The striking change in the dielectric constant results in an extremely reduced solubility of solute resulting into supersaturation in the solution and thus nucleation and growth of crystal takes place. The low dielectric constant of water allows the dissolution of organic compounds in the supercritical water. Similar tendency has been also observed for solvothermal systems. Non-aqueous phase organic solvents have been extensively used in the solvothermal synthesis. The organic solvents such as methanol, 1, 4-butanediol, toluene, and amines are usually used in the solvothermal route. The solvothermal synthesis can be processed at comparatively lower temperature and pressure as compared to the hydrothermal approach. Moreover, sensitive precursors to water can be easily tackled into solvothermal route. However, morphology and crystal phase of the prepared compound can be easily tailored through this route [107].

12.4.1 Synthesis of Nanomaterials via Hydrothermal and/or Solvothermal Approaches

Nanomaterial with manageable morphology, size, crystallinity of particles, and easy way of surface functionalization has attracted widespread research courtesy due to their unique optoelectronic, magnetic, and thermo-mechanical properties. Nanomaterials possess high surface to volume ratio in particles, and quantum confinement effect in semiconductor mainly governs the properties of the nanomaterials. In quantum confinement effect, the particle sizes are squeezed below to its Bohr radius. In order to synthesize the nanomaterials, the hydrothermal and/or

solvothermal synthetic routes are reflected as the most favorable tactics. In these techniques, controlled shape and size of particles, and exceedingly crystalline with high yield of nanomaterials at low cost is produced. Furthermore, these routes can be interconnected with MW to get the high quality nanocrystals with enhanced reproducibility.

12.4.2 Metal Oxides NPs

Metal oxide NPs are significantly useful materials due to their exceptional properties. These metal oxide NPs are typically utilized in a variety of research fields such as in catalysis, ceramic, optoelectronics, and so forth. In solvothermal technique, smaller size metal oxide NPs are prepared at comparatively lower temperature as compared to its hydrothermal approach [108]. Various metals oxides NPs such as Al_2O_3, CuO, γ-Fe_2O_3, $CoFe_2O_4$, CeO_2, NiO, ZrO_2, TiO_2, $BaTiO_3$, and $SrTiO_3$ are synthesized via hydro- and/or solvothermal approaches. Furthermore, the hydrothermal and solvothermal approaches are employed for the synthesis of $ZnGa_2O_4$, $BaZrO_3$, and $LiNbO_3$ [107, 109]. Persistent luminescence properties of Cr doped $ZnGa_2O_4$ have been reported for the hydrothermally synthesized sub 10 nm particles [110]. TiO_2 is widely studied metal oxide NPs for its photocatalytic properties. The oxide NPs prepared via these routes exhibit high crystallinity, precisely controlled particle shape, size which determines their advanced applications. Semiconductor metal chalcogenides nanomaterials are widely used in optoelectronic devices and in photovoltaic. The chalcogenides nanometrials comprised of ZnS, ZnSe, ZnTe, CdS, CdSe, CdTe, CuInSe, $Cu_{2-x}Se$, $AgInS_2$, and $AgGaS_2$ are reported via hydrothermal approach [107]. Ultra-small ($\sim$4 nm) hexagonal ZnS nanosphere has been synthesized using tetra-pyridine–di-thio-cyanato-zinc precursor into ethylene glycol via solvothermal route. During the synthesis, the increase in reaction temperature (160, 180, 200 °C) fetch bigger size ZnS nanospheres (200, 350, and 450 nm) [111]. Solvothermal synthesis of monodispersed Mn-doped ZnS nanospheres is reported. During the synthesis, $ZnCl_2$, $MnCl_2$, and sulfur powders are used as the precursors in oleic acid [112]. The hydro-solvothermal route has been further extended to synthesize ZnSe nanocrystal in form of quantum dots, nanorods, nanoplates, and in bulk form. ZnSe as well as ZnTe NPs are prepared through a solvothermal technique. During the synthesis, less toxic metal precursors are utilized as compared to the conventional chemical vapor deposition technique. The metal precursors $Zn(CH_3COO)_2$, $ZnSO_4$, and/or Zn powders, Se, Te powders and/or Na_2SeO_3, and Na_2TeO_3 are used as Zn, Se, and Te sources during synthesis. The frequent solvents used during the synthesis generally contain ammonia, triethylamine, ethylenediamine, and hydrazine as well. The pH of the reaction mixture is maintained at $\sim$10 [107, 113]. Highly ordered CdS sphere is synthesized via solvothermal route using $Cd(NO_3)_2$ as metal precursors, thiourea as S source, while polyvinylpyrrolidone (PVP) functions as a capping agent. Surfactant PVP provides the needed nucleation sites during nanocrystal growth. Higher concentration of PVP

entails more accessible nucleation sites promotes the NPs growth and consequently leads to small size NPs. This method has been also extended for the preparation of other sulfides like HgS, Ag_2S, and Bi_2S_3. During the hydrothermal and/or solvothermal synthesis of CdS NPs, thioglycolic acid and dithioglycol have been used as S sources [107, 114]. The compounds based on nitrides, arsenides, and phosphide having direct band-gap semiconductors are extensively applied in light emitting diodes, lasers, photo-detectors, optical amplifiers, etc. In light emitting diode (LED) application, commercially available GaN chip is used for illumination purpose [115]. Xie and his co-workers first reported the solvothermal synthesis of GaN compound. Polycrystalline GaN has been synthesized via solvothermal route using $GaCl_3$ and Li_3N precursors in benzene at 280 °C for 6–12 h. The absence of quantum confinement in GaN is attributed to its large size (∼32 nm) as compared to its Bohr exciton radius (∼11 nm). The innovative benzene solvent tactics has been executed at relatively lower temperature than that of traditional routes [116]. Moreover, GaN NPs have been synthesized using anhydrous ammonia as a solvent. Anhydrous ammonia has been condensed in a quartz tube containing the reactants Ga metal, GaI_2, and/or GaI_3 as Ga sources while NH_4I, NH_4Cl, or NH_4Br are added to produce the GaN. During the ammonia thermal synthesis of GaN, temperature plays a decisive role. Cubic phase amorphous GaN can be prepared when the growth temperature is ∼300 °C. When growth temperature is kept at 440 °C, hexagonal phase GaN is obtained [117]. Furthermore, other metal nitrides such as NbN, ZrN, HfN, and Ta_3N_5 are synthesized using $NbCl_5$, $ZrCl_4$, $HfCl_4$, and $TaCl_5$ as the metal precursor along with $LiNH_2$ as the nitriding reagent. By using benzene solvothermal reaction, highly crystalline Ta_3N_5, ZrN, HfN, and NbNNPs of changeable sizes can be synthesized [118].

12.4.3 Hydrothermal Treatment for Hollow Structures

Hollow structured nanomaterials such as hollow carbon sphere and mesoporous carbon spheres are of prime interest and widely applied in catalysis, bio-imaging, and drug delivery, lithium-ion batteries, fuel cells, sensors, etc. [119]. Low temperature hydrothermal approach is further used for the preparation of carbonaceous NPs. Highly biocompatible as well as economically viable precursors such as sugar, glucose, cyclo-dextrins, fructose, sucrose, cellulose, and starch have been used during hydrothermal synthesis of carbon NPs [120]. Generally, hydrothermally synthesized carbon NPs are spherical in nature. Reaction temperature plays a decisive factor in formation of carbon spheres. Carbon spheres of different diameter ∼0.2, 0.5, 0.8, 1.1, and 1.5 μm are produced using 0.5 M glucose as the carbon source and setting the reaction time and temperature of 2, 4, 6, 8, and 10 h and 160 °C, respectively. Growths of these NPs are consequence of dehydration, condensation, polymerization as well as aromatization processes. The reaction temperature range generally occurs from 150 to 350 °C, while synthesis time is generally set in between 4 and 24 h. Based on the precursors used during the

synthesis, the diameters of the synthesized NPs may diverge from 100 nm to few microns. The hollow carbon NPs have been synthesized using mesoporous or nonporous silica templates. Ultimately, selective etching of carbon NPs deposited onto mesoporous and/or nonporous silica templates promotes the formation of hollow carbon spheres (shown in Fig. 12.6) [121].

Wet aptitude of the surface of templates plays an extremely vital role. When the surface of the templates is not wetted by the precursor, then nonporous carbon NPs is obtained. Likewise, this route is comprehensively used for the synthesis of composite carbonaceous NPs. The composite carbonaceous NPs can be prepared via simple mixing of the metal precursors such as Ag, Pd, Se, and/or metal oxides as Fe_3O_4 and SnO_2 with a carbon source [122]. Silicon and germanium are significant semiconductor metals mainly due to their vast applications in optoelectronic devices. In order to synthesize crystalline silicon and germanium NPs via

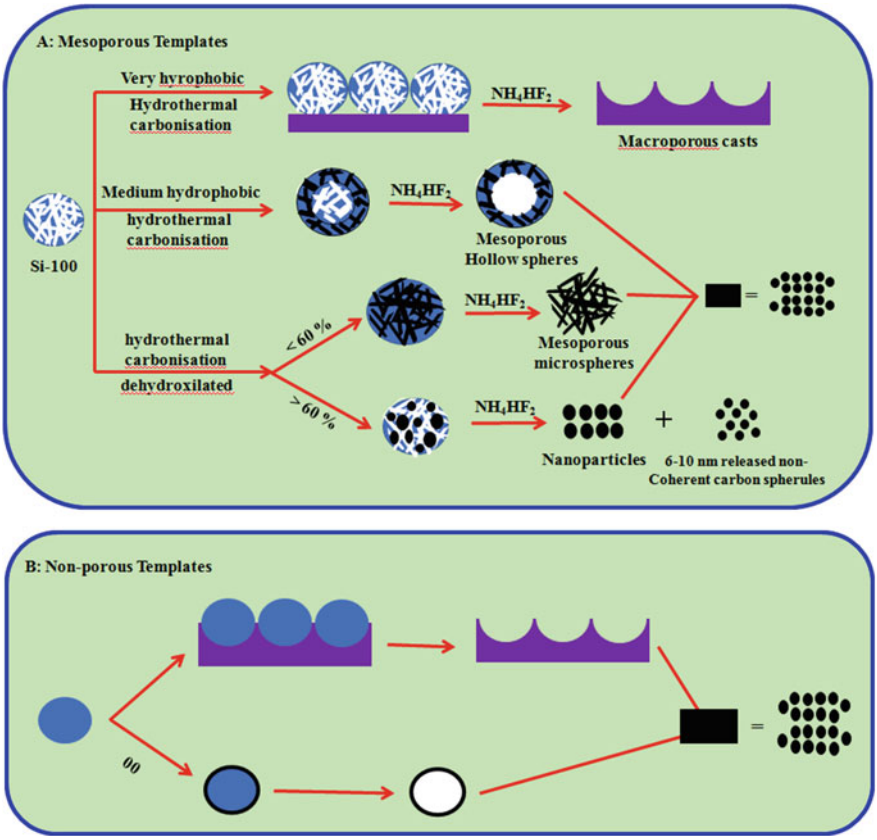

Fig. 12.6 (A) and (B) represent the schematic representation of the hydrothermal carbonization process using silica templates with different polarities, resulting in the formation of various carbon morphologies. This is redrawn from Refs. [120, 121]

hydro- and/solvothermal approach, a very high reaction temperature is kept. Solvothermal decomposition of tetra-ethyl germanium results the formation of the reduced crystallinity of germanium NPs. The decomposition can be executed at higher temperature in the presence or absence of surfactants into organic solvents and/or super-fluidic solvents such as CO_2. The surfactants involved during synthesis lead the nucleation and crystal growth via reverse micelles formation. Also surfactants permit not only the precise control over the morphology of the germanium NPs, but also stabilize the synthesized NPs [123]. Germanium nanocubes of 100 nm edge length via hexane solvothermal route have been prepared using heptaethylene glycol monododecyl as a surfactant. The same molar ratio of $GeCl_4$ and phenyl-$GeCl_3$ is employed as germanium precursors. Herein, Na metal sprinkled in toluene is used as the reducing reagent. The reaction mixture has been heated at 280 °C for 72 h in a hydrothermal reactor. Highly crystalline as-prepared germanium nanocubes with diamond cubic structure is observed. The synthesized germanium nanocubes consist of multi-slighter nanocubes that are linked to the surface-adsorbed surfactant NPs [124]. When the surfactant is replaced by pentaethylene glycol ether, a combination of spherical, triangular, and hexagonal Ge NPs is observed (diameters ~15 to 70 nm). By adjusting the surfactant amount, the shape of germanium NPs can be tailored. The germanium spheres with average diameters of the range ~6 to 35 nm have been obtained for the decreased volume of surfactant ~1.8 to 0.6 ml. The yield of the germanium NPs is mostly influenced by the reaction time period. Prolong heating time during solvothermal treatment of the reaction mixture ~4 to 12 h increases the yield of the product. On the other hand, the size and crystallinity of NPs does not depend on the reaction time. It is due to the presence of the capping reagents into the reaction medium. In the similar fashion, solvothermal approach is also employed for the synthesis of Si NPs [107].

12.4.4 Metal Nano-particles Synthesis via Hydro/ SolvoThermal Routes

Metallic NPs exhibit numerous fascinating properties, namely optical, electronic, magnetic, etc. Using these unique properties, these NPs have been applied in diverse area of research such as in catalysis, sensors, and memory devices. By using wet chemistry routes, controlled shape-size synthesis of metal NPs is obtained via suitable use of reducing and capping agents. Moreover, precise control over NPs and crystallinity is poor. Hydrothermal and/or solvothermal routes assure superior control over morphology and crystallinity as compared to wet-chemical routes. Ultra-small ~1.7 nm Pt NPs are prepared by employing an ethylene glycol solvothermal route in basic medium. Here, ethylene glycol acts as solvent as well as a reducing agent. $H_2PtCl_6{\cdot}6H_2O$ is used as Pt metal precursor during synthesis. The reaction mixture temperature is kept at 160 °C for 3 h [125]. The EG solvothermal route is further extended for the preparation of Ag NPs. In a typical synthesis of Ag

NPs, $AgNO_3$ is added into suitable amounts of toluene, EG, and dodecylthiol and kept in the reactor at 160–170 °C. The prepared Ag NPs exhibit an ordered spherical shape (average diameter ~10 nm). Thiol used during the synthesis acts as a complexing reagent, while ethylene glycol functions as reducing agent. By adjusting ethylene glycol to thiol ratio ~3 to 1.5, the morphology of the Ag NPs shows remarkable change in the morphology. Ag NPs show spherical to rectangular shape morphology with a somewhat decreased diameter ~6 to 10 nm [126]. DMF solvothermal approach has been employed to grow Ag and Au NPs. In addition to EG and DMF, other reducing agents such as $NaBH_4$, N_2H_4, NH_2OH, and ethanol have also been used to prepare metal NPs [127]. DMF solvothermal method has been utilized for the synthesis of Pt-Ni alloy system. Platinum (II) 2,4-pentanedionate and nickel (II) 2,4-pentanedionate are used as precursors for Pt and Ni metals, respectively. During the synthesis, 30 mM $Pt(acac)_2$ and 10 mM $Ni(acac)_2$ concentrations have been dissolved in DMF. The reaction mixture has been placed in an electrical furnace at 200 °C for one day. Temperature below 200 °C, decomposition of $Ni(acac)_2$ has not been completed, as-prepared platinum-nickel alloy NPs show high crystallinity. The average diameter of alloy NPs is ~10–13 nm. By tuning the metal precursors ratio, different sizes NPs are obtained for the bimetallic Pt–Ni alloy. The similar approach can be utilized for the synthesis of Pt–Co and Pt–Fe bimetallic alloys NPs [107].

12.4.5 Metal Organic Framework (MOF) NPs

MOFs are promising functional nanomaterials which attracted a great deal of attention owing to their potential applications in hydrogen storage, catalysis, bio-imaging, drug delivery, sensors, etc., gas separation and proton exchange membranes, etc. MOFs consist of a chain of hybrid nonporous crystalline nanomaterials comprised of metals and organic linkers with pore sizes of ~0.4 to 6 nm [128–131]. MOFs are usually prepared through hydrothermal and/or solvothermal routes. Gentle temperature and pressure are used during MOF NP synthesis to keep away from decomposition of organic ligands. MOF NPs for biomedical use are highly demanding. The surfactant free MOFs NPs growth is performed via an easy solvothermal route. Solvothermal synthesis of Fe(III) MOF NCs with an organic framework Fe3-(μ3-O)$Cl(H_2O)_2(BDC)_3$ has been prepared via taking equal-molar $FeCl_3$ and BDC in DMF under MW heating at 150 °C [132]. The MW heating promotes smaller NPs. The NPs thus obtained are highly crystalline octahedral with an average diameter ~200 nm. Furthermore, MOF NPs are targeted and functionalized with dye molecules for cellular imaging. Also, these MOFs can be used as anticancer pro-drugs for tumor therapies. Though these functionalized NP_S are not stable in a physiological atmosphere, post-synthesis coating of the MOF NPs with silica layer resolves the stability issue. Surfactant-assisted hydrothermal synthesis has been employed under the presence and absence of microwave heating to synthesize the paramagnetic Gd(III) MOF NPs. As-synthesized MOF NPs show

high crystallinity. When the reaction is carried out at room temperature, only amorphous GdMOF NPs can be obtained because the nucleation rate is too rapid and dominates the NP growth. The MOF NPs obtained under microwave heating have a formula of $[Gd_2(bhc)(H_2O)_6]$ MOF NPs. The synthesized Gd(III) MOFs can be applied to magnetic resonance imaging [133]. Similar hydrothermal approach has been utilized to synthesize Tb (III), Eu (III), and Mn(II) MOF NPs. MW heating, temperature of reaction mixture, and ratio of water to surfactant ratio impart the noteworthy effects over morphology of the synthesized MOFNPs. Lower synthesis temperature and a higher ratio of water to surfactant lead to the development of nanorods, while greater temperature and MW heating promotes the formation of shorter nanorods or octahedral NPs [107].

12.5 Sonochemical Synthesis

Nanostructured materials open a new realm of diverse applications such as optoelectronics, catalysis, sensing, water splitting, and in medical diagnostics. Nanomaterials exhibit distinct properties as compared to its bulk. The characteristics of the nanostructured materials are heavily dependent on synthesis process by which they have been prepared. Therefore, it induces an interest among the materials scientists to develop the easily adaptable synthesis methodologies to prepare the varieties of nanostructured materials. Among the various synthesis route available such as photo and wet chemistry, hydrothermal and flame pyrolysis for the materials synthesis, ultrasound-based nanomaterials gained a lot of attention for its multi-dimensional applications [134]. Ultrasonic wave serves as an efficient energy source for synthesis of organo-metallic and inorganic materials which found their profound applications in organo-metallic chemistry and industrial manufacturing [135]. This synthesis approach provides high temperature as well as high-pressure synthesis conditions. It covers a vast range of reaction condition which is not feasible with other pre-existing techniques. Sonochemistry involves the utilization of ultrasound energy with frequency (ν) range $\sim$15 kHz to 10 MHz. This approach provides unique pathways to prepare the compounds in a simple and easily accessible at high temperature and pressure. Ultrasonic waves predominantly cause cavitation in an aqueous medium followed by formation, evolution, and breakdown of micro bubbles. An ultrasonic energy initiates the formation and growth of bubbles to a solution containing chemical precursors followed by diffusion of the precursor vapor. After reaching the bubble size to its critical limit, the bubble collapses and generates shockwaves.

At specific conditions, overgrowth of a micro bubble can take place and later breakdown which finally liberating the energy deposited in the bubble at a very short time duration. The chemical reaction process takes place under fast heating and cooling rate $>10^{10}$ K s^{-1}. The cavitational collapse leads to a very high temperature (5000 K) and pressure (1000 bar). This collapse process is almost adiabatic in its preceding stages which are mainly accountable for the extreme

environments representative of sonochemistry [136]. Remarkably, such unusual environments are not resulting straightway from ultrasound since acoustic wavelengths have far longer value as compared to the molecular sizes. Therefore, there is an absence of any straight molecular-level interface between ultrasound and the elementals pieces. The phenomenon of acoustic cavitation occurs via development, evolution, and implosive breakdown of bubbles in liquid phase. The cavitation process under highly intense ultrasound is accountable for the chemical effects of ultrasound [137]. Under ultrasound irradiation, sinusoidal expansion and compression of acoustic waves form the cavities and allow the bubble oscillation. The oscillating bubbles collect the ultrasonic energy and finally grow to a critical size. Under these thrilling environments, emission of light occurs. The emission of light under sonochemical irradiation is termed as sono-luminescence [138]. The reaction involved in ultrasonic system comprised of a power source, a piezoelectric transducer with electrodes, a Ti horn bearing stainless steel collar, reaction mixture container, and a bath chamber. Highly intense ultrasonic titanium horn with piezoelectric transducer is preferred for the lab-scale sonochemical reactions (Fig. 12.7). Ultrasonic horn provides 10–100 W acoustic powers during sonication to the liquid solution. The cavitation procedure happens over a wide spread range of frequencies (10 Hz to 10 MHz). The common alternate to ultrasonic horn in the synthesis set up into laboratory, and ultrasonic cleaning baths are used. The power density of ultrasonic cleaning baths is governed by a small input power as compared to power produced by an ultrasonic horn. Cleaning baths are frequently trivial for many sonochemical reactions. Moreover, it can be helpful for the study of the substantial effects of ultrasound on very reactive metals such as lithium or magnesium producing emulsions which promotes the suspensions of solids and exfoliating layer structured nanomaterials.

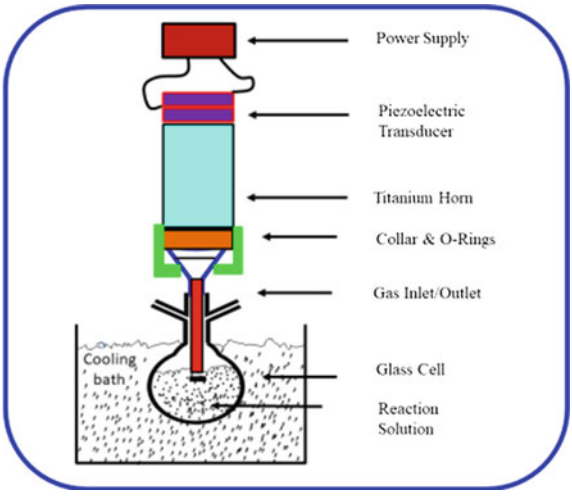

Fig. 12.7 Typical high intensity ultrasonic set up for nanostructured synthesis. This is redrawn from references [136–138]

Metal, metal oxide, sulfide, and alloy NPs are prepared by sonochemical synthesis approach using aqueous and non-aqueous solutions. The structural, optoelectronic, magnetic, and electrochemical assets of metallic NPs have the emphasis of contemporary research accomplishments. Under sonochemical route synthesis, particle undergoes to exhibit different morphologies such as spherical, rod, wires, hollow, layered type structure 2D materials, etc. [139].

12.5.1 Metal NPs Synthesis via SonoChemical Route

In literature, sonochemical synthesis of nanostructured metallic noble NPs as Au, Ag, Pt, and Pd is explored. The sonochemical reduction of noble metal salts has advantages above other existing old-fashioned reduction methods such as sodium boro-hydride, hydrogen, and alcohol, etc. In this synthesis, involvement of reducing agent is not required. Hence, the reaction rates during the synthesis are rationally fast which finally leads to the formation of metal NPs [140–142]. The water molecules under sonolysis generate $H^{\bullet}$ radicals which function as reductants. Moreover, 2-propanol as organic additive is incorporated to generate a secondary radical species. The secondary radical species can considerably endorse the reduction rate. The detailed process of metal preparation via sonochemical route has been demonstrated as [140]:

$$H_2O \rightarrow H\cdot + OH\cdot \tag{12.1}$$

$$H\cdot + H\cdot \rightarrow H_2 \tag{12.2}$$

$$H\cdot + OH\cdot \rightarrow H_2O \tag{12.3}$$

$$RH + OH\cdot (\text{or } H\cdot) \rightarrow R\cdot + H_2O \text{ or } (H_2) \tag{12.4}$$

$$OH\cdot + OH\cdot \rightarrow H_2O_2 \tag{12.5}$$

$$\text{Au (III)},\ \text{Ag(I)}, \text{Pt (III)}, \text{Pd (III)} + H\cdot \text{ or } R\cdot \rightarrow \text{Au(0)},\ \text{Ag(0)},\ \text{Pt(0)},\ \text{Pd(0)} \tag{12.6}$$

$$nM(0) \rightarrow M_n(M = \text{Noble metal}) \tag{12.7}$$

The sonochemical reduction of noble metals involved tedious reduction process. The consequence of several factors, namely time, concentration, and ultrasound frequency, with diverse organic additives to control shape, and size of particles has been reported. It is reported that particle size obtained during sonolysis is inversely reliant on alcohol concentration as well as alkyl chain stretch. It has been thoroughly linked to the circumstance that alcohols adsorbed on the surface of metallic NPs stabilizes and furthermore confine the nucleation rate [140]. Highly

monodispersed gold nanodecahedra under ultrasonic irradiation with elevated yield and markedly enlarged reproducibility is reported. Gold nanodecahedra is obtained via sonochemical reduction of $HAuCl_4$ over already synthesized gold seeds into DMF solution. Unexpectedly, in the absence of ultrasound, inferior yield of gold nanodecahedra by elevated polydispersity is observed via thermal reduction [143, 144].

An analogous synthesis method has utilized for the preparation of silver nanoplates. The ultrasound-assisted Ostwald ripening procedure promotes the development of silver nanoplates via silver NPs produced at an initial stage of reaction [145]. The synthesis of Pd and Pt NPs via reduction of K_2PdCl_4 and H_2PtCl_6 precursors under sonochemical approach has been reported. The consequence of inert atmosphere on the particle size of Pd and Pt NPs has been reported. Under the Ar atmosphere, particle size of Pd is observed to be 3.5 nm, while its size is 2 nm in presence of N_2 atmosphere. Comparatively, narrower sizes of Pt NPs are obtained under Xe atmosphere. This was mainly due to the acoustic cavitation leading to formation of hot spot temperature [146]. Also, highly stable Pd NPs are prepared via ultrasonic irradiation (frequency 50 kHz for three hours) to $Pd(NO_3)_2$ solution into ethylene glycol and PVP. Ethylene glycol reduces Pd(II) to metal Pd while co-ordination of Pd atom to the carbonyl functional group of PVP promotes the steadiness of Pd NPs [147].

Fe_3O_4 magnetic NPs are synthesized by sonochemical route. Iron pentacarbonyl and polyethylene glycol have taken together in hexadecane. The decomposition of $Fe(CO)_5$ occurs in the presence of polyethylene glycol, and monodispersed ultra-small NPs $\sim$3 nm particles are obtained. The reaction was carried out in dark condition. The presence of a black slurry in reaction vessel leads to $Fe(CO)_5$ decomposition [148].

12.5.2 Metal Chalcogenides

Metal sulfide NPs show emerging character owing to their extensive use in miscellaneous fields such as lasers, optoelectronic, thermoelectric devices, and in infrared spectroscopy cells. The nano-crystalline metal chalcogenides exhibit superior performance as compared to their bulk counterparts. Bismuth sulfide nanorods are synthesized through a facile sonochemical method using bismuth nitrate and sodium thiosulfate in an aqueous solution. Different complexing agents such as triethanol amine, sodium tartrate, and ethylenediamine tetra-acatetic acid are used during synthesis. These complexing agents promote the different diameter and length of Bi_2Se_3 nanorods [149].

In another report, hexagonal phase cadmium sulfide and cadmium selenide NPs are observed using cadmium acetate as metal precursor. The NPs have been obtained under reduced atmosphere H_2/Ar(5/95) via ultrasonication. The hydrogen used during the reaction process acts as reducing agent, while high temperature is attained via collapse of bubbles followed via reduction of precursor [150].

Similarly, synthesis of PbSe and ZnSe NPs using sonochemical technique has been reported by Gedanken and his co-workers [151].

Metal selenides demonstrate extensive applications in diverse field such as in optical filters, optical recording materials, photovoltaic, sensors as well as laser materials [152]. The CdSe semiconductor nanocrystal finds its profound application in photoconductor. Hollow sphere of CdSe via sonochemical approach has been reported. Uniform and regular spheres of CdSe nanocrystal with average diameter of ~120 nm are obtained [153]. Ultrasonically synthesized hexagonal CdSe nanocrystals are reported using cadmium acetate and metal selenium in a reduced atmosphere of H_2/Ar. The precise experiments demonstrate that the hydrogen used here functions as a reducing agent. An extremely extraordinary temperature is attained through the bubble breakdown which accelerates the reduction of Se [154]. HgSe is an important semiconductor material which is utilized in photoconductors, solar cell, IR detector, tunable lasers, etc. At room temperature, HgSe is prepared under ultrasonic irradiation using mercury acetate and sodium selenosulfate in aqueous phase. The HgSe NPs with various sizes are obtained using the complexing agents such as ethylenediamine (EDA), ammonia, and tri-ethanolamine (TEA). The high concentration of TEA promotes the growth of tiny particles [155]. A range of metal chalcogenides such as MoS_2, Cu_3Se_2, Cu_7Te_4, Cu_4Te_3, $AgBiS_2$, etc., have been synthesized via sonochemical approach. During the typical ultrasonic synthesis, these metal chalcogenides necessitate the metal precursors into aqueous solution, and a chalcogen source such as thiourea is used for sulfur, while selenourea is used for Se sources. Under ultrasonic irradiation, in situ generation of H_2S or H_2Se reacts with metal salt precursors in aqueous phase to generate metal chalcogenide NPs [156–159].

12.5.3 Metal Carbides

Sonochemical approach has been further extended for the preparation of metal carbides such as Fe_3C, PdC, Mo_2C. At room temperature, PdC NPs are synthesized via the reduction of $Na_2PdCl_4$with interstitial carbon in aqueous solution. The concentration of carbon in Pd particles has been optimized by altering the nature and the concentration of organic additives. The PdC synthesis is composed of firstly formation of Pd cluster growth during Pd nanoparticle formation. In second step, organic additives have been adsorbed onto Pd cluster, and lastly, diffusion of carbon atoms takes place into Pd metal lattice. Higher carbon chain such as hexanol, ethanol, methanol, and precise concentration of isopropyl alcohol (IPA) promotes the enormous number of C atoms in Pd metals [160]. Iron carbide NPs have been prepared via sonochemical approach using Ferrocene $Fe(C_5H_5)_2$ as a metal precursor. The absence of oxygen in the precursor prevents the formation of Fe_3O_4NPs. Amorphous phase iron carbide is obtained via sonolysis of ferrocene in diphenylmethane. The modifications of reaction parameters such as ultrasound frequency, tip diameter, and immersion depth throughout the experiment promote

the formation of monodispersed nanoparticles ~6 to 12 nm [161]. For the preparation of molybdenum carbide NPs, first slurry of molybdenum hexacarbonyl is prepared through ultrasonication (operating frequency ~20 kHz). Here, hexadecane is used as a solvent because it has small vapor pressure. The acquired nanomaterial shows porous character with aggregate of 2 nm sized Mo_2C NPs [162].

12.5.4 Bimetallic NPs/Metal Alloys/Metal Composites

Sonochemical route has been implemented for the synthesis of colloidal bimetallic NPs. Bimetallic NPs have shown the fruitful application as catalyst as well as in optoelectronic device applications. Suslick and his co-workers for the first time revealed the utilization of ultrasound to produce bimetallic NPs [163, 164]. Bimetallic NPs composed of gold and palladium is reported using sonochemical synthesis. Ultrasonic irradiation promotes the reduction by sodium dodecyl sulfate (SDS) of Au (III) and Pd (II) ions from $NaAuCl_4 \cdot 2H_2O$ and Na_2PdCl_4 in an aqueous medium. The surfactant SDS used here improves the reducing rate as well as the stability of the nanomaterials. The obtained nanocrystals exhibit the spherical shape particles with diameter ~8 nm [165]. An outstanding soft magnetic property has been reported for an amorphous phase ferromagnetic alloys comprised of Fe and Co. The boosted magnetic behavior of alloys has been used in magnetic data storage as well as in power transformers [166]. Furthermore, sonochemical decomposition synthesis is employed for the preparation of amorphous phase alloy of $Co_{20}Ni_{80}$ and $Co_{50}Ni_{50}$. The explosive organic metal precursors such as $Co(NO)(CO)_3$ and $Ni(CO)_4$ in decalin are utilized at 273 K under argon pressure (100–150 kPa). Synthesized alloys NPs exhibit superparamagnetic behavior [167]. Under ultrasonic irradiation, the Fe/Co alloy is synthesized using $Fe(CO)_5$ and $Co(NO)(CO)_3$ precursors in diphenylmethane solution in an inert argon atmosphere. The NPs having a metal alloy core along with a coated shell are obtained. The alloy NPs reveal exceptional storage constancy with magnetic performance [168]. Pt–Ru bimetallic system has been extensively applied in catalysis as well as in fuel cells. The colloidal synthesis of Pt–Ru bimetallic NPs in an aqueous phase has been obtained via sonochemical reduction of Pt(II) and Ru(III). The synthesis is executed at the ultrasound frequency ~210 kHz, while temperature is set to 20 °C. By the use of SDS as a stabilizing as well as capping agent, particle size of 5–10 nm NPs is obtained. Furthermore, using PVP, ultra-small bimetallic NPs in the range of ~5 nm are obtained [169].

12.5.5 Metal Oxide NPs

Metal oxides display a vigorous character in the arena of interdisciplinary branch of sciences, namely physics, chemistry, and materials science. In the technological point of view, these metal oxides exhibit profound applications such as in sensor, fuel cells, piezoelectric devices, microprocessors and microelectronic circuits, etc. Moreover, these metal oxides are employed in catalysis and as surface coating to prevent the corrosion as well. Owing to their vast range applicability, the synthesis of these metal oxide NPs has drawn much attention to the research community. Mesoporous tin oxide SnO_2NPs have been reported via sonochemical method using tin ethoxide as a precursor and CTAB as surfactant which controls its structural morphology [170]. The synthesis of lanthanide metal oxides such as Y_2O_3, Er_2O_3, CeO_2, Sm_2O_3 and La_2O_3, via sonochemical route has been also reported. These metal oxides are synthesized via nitrate salts of the corresponding rare earth metal ions as precursors, SDS as surfactants and urea as a precipitating reagent, respectively. Molar ratio of rare earth metal ions, SDS, and urea (1:2:30) is maintained during the synthesis [171]. Surfactant free zinc oxide nanoparticles are prepared via sonochemical route using zinc acetate and 1,4-butanediol. During synthesis process, 1,4-butandiol functions both as solvent and capping agent. For desired product formation, reaction is executed under ultrasonic irradiation [172]. The shape-selective ZnO NPs synthesis via sonochemical route is reported. The prepared ZnONPs exhibit different shapes such as nanorods, nanocups, nanodisks, nanoflowers, and nanospheres. It is observed that precursor concentration, power density of ultrasonic source, sonication time, kind of hydroxide anion mediators, and the capping agent are crucial aspects in the shape-selective ZnO nanomaterial preparation [173]. Furthermore, other metal oxides TiO_2, CeO_2, MoO_3, V_2O_5, In_2O_3, $ZnFe_2O_4$, $PbWO_4$, $BiPO_4$, and $ZnAl_2O_4$ have been successfully synthesized. Sonochemically prepared titania nanoprticles show superior photocatalytic activity to commercially available Degussa P25. The improved photocatalytic activity is ascribed to the highly crystalline nature of titania generated by rapid hydrolysis via ultrasound irradiation [174–181].

12.5.6 Sonochemical Preparation of Hollow and Layered Structures

The deposition of inorganic NPs on solid substrates such as silica or carbon nanotubes via sonochemical approach is employed to obtain hollow nano-structures. Hollow spheres of MoS_2 and MoO_3 have been reported via sonochemical technique [182]. MoS_2/SiO_2 composite under ultrasonic irradiation is obtained using isodurene slurry of molybdenum hexacarbonyl, sulfur, and silica nanospheres under an inert Ar atmosphere. Analogous process is carried out in the presence of air, and the absence of sulfur promotes the formation of a MoO_3/SiO_2 nano-composite.

Successive HF treatment leaches out the silica spheres which results in the formation of MoS_2 and MoO_3 hollow spheres. (Fig. 12.8 a, b and c). Remarkably after heat treatment, hollow MoO_3 nanospheres exhibit hollow single crystal (Fig. 12.8d).

Sonochemical synthesis of hollow hematite has been reported. During the synthesis, carbons NPs are utilized as an instinctively detachable template. The mechanism behind the formation of the hollow hematite formation is employed in situ combustion of the carbon NPs. However, sonochemical decomposition of Fe $(CO)_5$ resulting an amorphous iron NPs which form shells in the vicinity of carbon NPs. The fast oxidation of the high surface area iron shells under air exposure ignites the interior carbon particles. The combustion of the carbon NPs produces sufficient heat to crystallize the iron oxide shells consequently leads to hollow α-Fe_2O_3 cores [183]. Sonochemical synthesis of porous Co_3O_4 nanotubes has been reported. Carbon nanotubes (CNTs) have been utilized as a sacrificial template

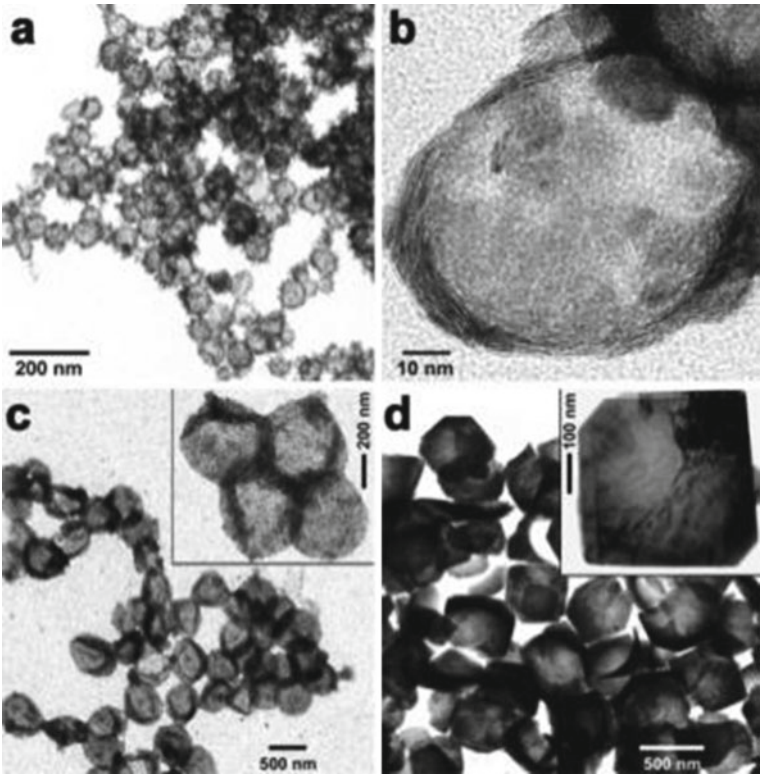

Fig. 12.8 TEM images of sonochemically prepared hollow MoS_2 nano-spheres **a** and **b** and hollow MoO_3 **c** after leaching of the silica template but before thermal annealing and **d** after thermal annealing and formation of hollow single crystals (**d**). Reproduced with permission from ACS publisher [182]

during the synthesis leads to the formation of CoO_x/CNTs composite. The nano-composite is further calcined into air to be on fire which finally removes the carbon nanotubes leads to porous nanotubes of CoO_x in Co_3O_4. The synthesized porous Co_3O_4 nanotubes act as an excellent electrode material employed in lithium batteries [184]. Hollow FePt spheres are reported via sonochemical deposition technique. Sonochemically synthesized FePt bimetallic particles are deposited on polyelectrolyte layers modified silica spheres. Consequent HF curing yields hollow FePt spheres. Fascinatingly, annealing of hollow FePt spheres exhibits magnetic properties with modified character from soft to hard magnet [185]. Polymer spheres such as polystyrene and poly-methyl-methacrylate are also used as a template material to create hollow structured materials [186]. In this situation, polymer cores are separated by either thermal pyrolysis or extraction with organic solvents from composites.

Ultrasound is proved to be formidable means for the chemical preparation of mono and multilayered graphene. The pristine graphite has been oxidized by Hummer's approach to synthesize the grapheme oxide. In grapheme oxide, inter-layer distance is increased as compared to graphite which results in weaker Vander Waals force. Subsequent to gentle sonication, single-layered graphene oxides have been synthesized that can be further reduced to graphene. The direct liquid-phase exfoliation of graphite via sonication gives the easy processing of graphene. In order to attain high yields of exfoliated graphene from graphite, the surface energy of the solvent must be equal to the surface energy of graphite (40–50 mJ m^{-2}). Sonication of graphite in appropriate solvents such as N-methyl-pyrrolidone (NMP)) promotes the formation of single layer and few layer graphene [187].

Ultrasound is repeatedly used to separate single-walled CNTs, which typically form bundles because of the presence of the Van der Waals force. This methodology has been utilized for the synthesis of other layered material such as $MoSe_2$, $MoTe_2$, MoS_2, WS_2, $TaSe_2$, $NbSe_2$, $NiTe_2$, BN and Bi_2Te_3. These materials have been exfoliated in the liquid phase to prepare monolayer nanosheets [188].

12.5.7 Sonochemical Preparation of Protein and Polymer Pano and Microstructures

Ultrasonic approach has been further transformed to synthesize biomaterial and polymers as well. The sonochemical synthesis of protein microspheres is obtained via sonication of a protein solution which contains serum albumins (Fig. 12.9).

Highly biocompatible and stable microspheres have meticulous attention in a variety of biomedical applications applied as contrast agents for MRI, sonography, optical coherence tomographym, and drug delivery carriers [189]. The collective effort from emulsification termed as a physical effect and cavitation corresponding to chemical effect consequently promotes the microsphere formation. The protein microspheres produced via ultrasonic emulsification attain significantly enhanced

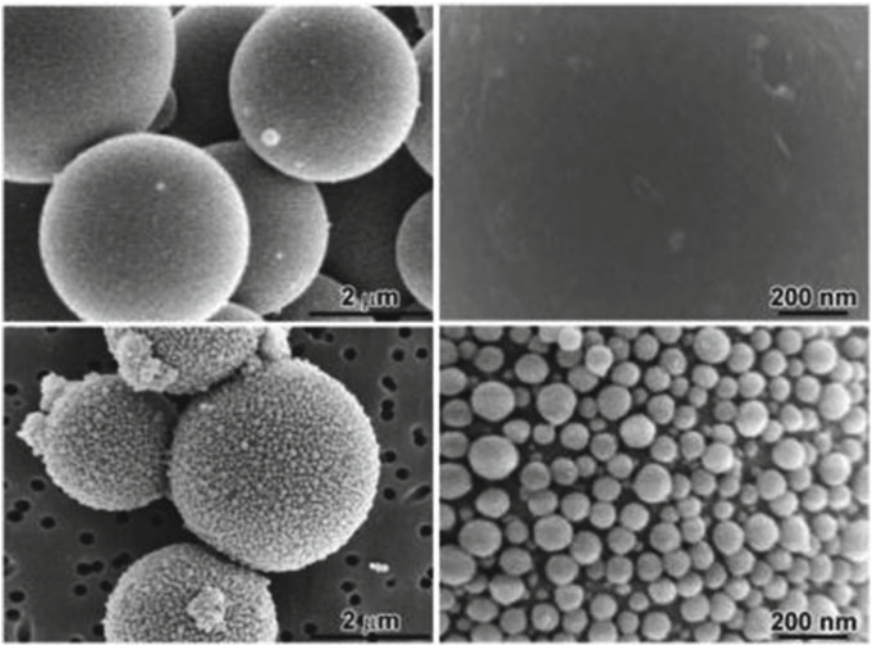

Fig. 12.9 SEM images of sonochemically prepared protein microspheres before and after nanoparticle functionalization by layer-by-layer adhesion: upper left, native microspheres as-prepared by sonication of bovine serum albumin and upper right, close-up of the surface; lower left, silica-coated microspheres using a RGD polylysinepeptide to reverse surface charge and lower right, close-up of its surface. Reproduced with permission from ACS publisher [189]

stability via covalent disulfide cross-linking of cysteine. Hydroperoxyl radicals are mainly generated, and these radicals are primarily accountable for this cross-linking [190, 191]. Hydroperoxyl radicals HO_2. generated during the sonolysis of water promotes induce cross-linking of the disulfide bonds linking with cysteine amino acid. The protein microspheres have been tailored via conjugation of selective cancer-cell ligands such as folate, RGD peptides, and mercaptoethane sulfonate to its surface [192].

12.5.8 Core @Shell Nanomaterials

An easy and effective sonochemical route has been employed for ZnO@CdS core@shell synthesis. ZnO nanorods is synthesized via oxidation of ZnO/Zn particles in air at high temperature [193]. In a typical synthesis process under ultrasonic irradiation, ZnO nanorods, cadmium chloride, and thiourea in an aqueous solution result the ZnO nanorods/Cds NPs formation [194]. Synthesis of Fe_3O_4@SiO_2 core@shell NPs via sonochemical route is reported [195]. It is observed that Fe(II)

and Fe(III) metal precursors get precipitated under ultrasonic irradiation which exhibit narrower Fe_3O_4 NPs size distribution as compared to precipitation obtained via mechanical stirring. It is reported that an alkaline TEOS hydrolysis into water alcohol mixture with Fe_3O_4 NPs increases the homogeneity and reduces the agglomeration of Fe_3O_4@SiO_2 NPs significantly. The thickness of silica shell is easily tailored under ultrasound irradiation. Core/shell hetero structured SnO_2@CdS has been prepared using SnO_2 nanobelt as a support. In the typical preparation, first CdS NPs are deposited over SnO_2 surface. The CdS NPs thus formed during the synthesis are of spherical type, and their sizes are in the order of 10–20 nm. Single crystal SnO_2 nanobelt having rutile structure is prepared via thermal evaporation metallic tin powders at 800 °C. In a typical synthesis process, SnO_2 nanobelts, cadmium chloride, and thiourea are mixed into 100 ml deionized water irradiated with ultrasound (100 W, 40 kHz) for 1–3 h [196]. Under ultrasound irradiation, the reduction of $AuCl_4^-$ ions to Au^0 (gold metal) and $AgNO_3^+$ ions to Ag^0 (silver metal) takes place in the presence of alcohols at room temperature [197]. Under ultrasound irradiation, cavitation takes place which generates primary and secondary radicals which reduces the gold chloride and silver nitrates into their respective metal ions. The presence of hydrogen atom along with alcohol radicals reduces the gold and silver ions to produce Au–Ag bimetallic core@shell NPs. It is also reported that in the presence of polymer, reaction of primary radicals with the polymer promotes the formation of polymeric radicals. It assists in reduction of the analogous metal ions to produce metal NPs [198, 199].

12.5.9 Ultrasonic Pyrolysis (USP)

Ultrasound produces chemical reactions in sonochemical synthesis. Moreover, in USP (ultrasonic pyrolysis), an ultrasound has not engaged directly during synthesis. Ultrasound acts as phase separator into one micro-droplet reactor to other. In sonochemical route, highly intense low-frequency ultrasound $\sim$20 kHz has been generally used; whereas in USP, high frequency $\sim$2 MHz with low intensity ultrasound is employed. Ultrasound is employed for nebulising the precursor solution which assist to generate micron-sized droplets during USP synthesis. Droplets thus generated by ultrasonic nebulisation have been heated under a gas flow before dispensed to chemical reaction. Large-scale production of ultrafine particles finds its utility in industry. Also, this technique is quite useful in film deposition. During this technique, creation of aerosols under ultrasonic nebulizer followed by thermal decomposition occurs [199, 200]. As compared to traditional techniques, USP has shown many merits such as easy and continuous operation, high purity reaction products, etc. This technique is equally applicable for small- and large-scale mass production with high reliability as well as reproducibility. Spherical NPs are prepared via the USP route. Liquid droplet formation takes place under ultrasonic nebulisation in USP route. In the USP process, firstly generated liquid droplets are subjected to the heated zone having Ar, N_2 and O_2 as carrier

gases followed by evaporation of solvents at droplet surface. The droplets rapidly contract and attain supersaturation after heating. The precipitation of solute takes place at droplet surface. Moreover, thermal decomposition can generate intermediate compounds in the form of porous or hollow structured particles [173]. In a typical USP experimental set up, a vessel having transducer at the base fixed with a mist connected to the tubular furnace. The collector chambers have been positioned at the furnace outlet (Fig. 12.10). The USP procedure requires droplet creation, diffusion of the solutes, evaporation of solvents, and precipitation followed by decomposition and densification (Fig. 12.10b). For the film deposition, silicon and glass substrates have been positioned inside the furnace.

USP technique is established as a multifaceted approach for the synthesis of fine powders of metals, metal alloys, and ceramic materials. For the synthesis of the metals NPs such as Ag, Pd, Au, Cu, Ni, Co, and their alloys as Ag–Pd, USP technique is extensively utilized. In order to prepare metal or alloys particles, generally it engages the USP decomposition of metal salt precursor solution in an

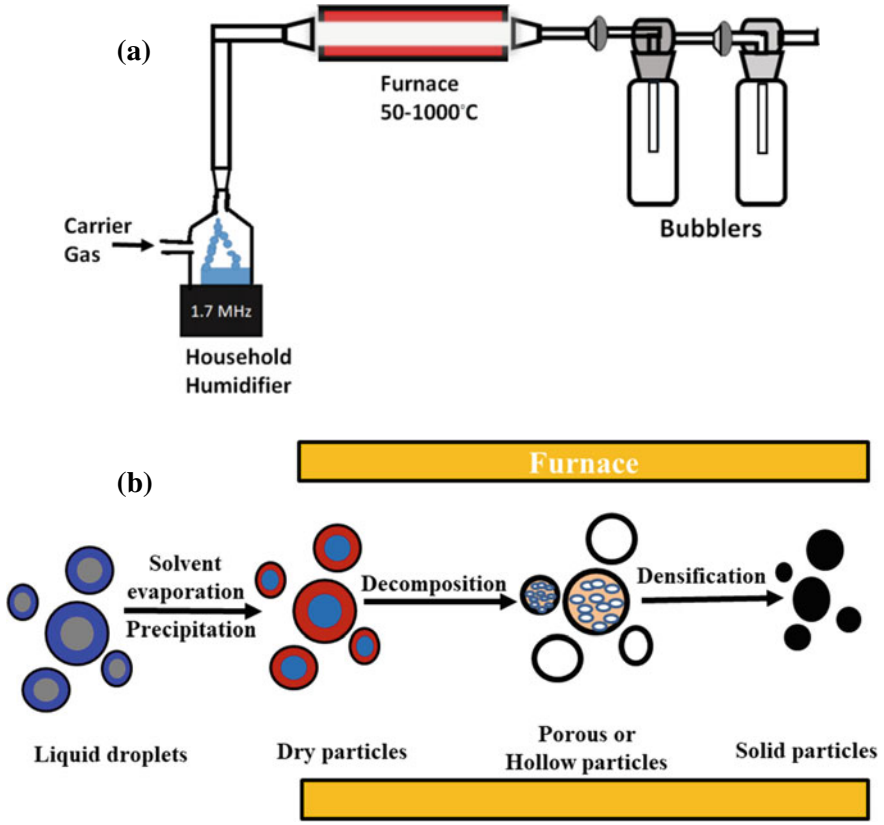

Fig. 12.10 Schematic illustration of **a** typical USP apparatus and **b** a schematic diagram of simplified USP process. This is redrawn from references [173, 199, 200]

inert atmosphere (N_2 or Ar flow) [201–206]. Highly crystalline nanowires of Zn, Cd, Co, and Pb nanowires are produced by USP route using methanolic solutions of corresponding metal acetates [207]. Micron-sized metal oxides and chalcogenides synthesis are reported via USP technique. During metal oxides synthesis, precursors of metal nitrates, chlorates, and acetates have been engaged; while for the preparation of metal chalcogenide, chalcogen sources are mixed into the precursor solution [140]. Suslick and Skrabalak employed silica as a sacrificial module to synthesize porous MoS_2 structure by USP approach. Silica NPs are tightly packed into an evaporating droplet and can afford an in situ nanostructure scaffold [208].

The exploitation of a silica template is more utilized for the preparation of metal oxides NPs. The USP preparation of diverse shapes of titania nanostructures, comprising porous, hollow, and ball-in-ball architectures has been reported. Silica-titania composite porous titania as well as silica-titania composite covered with cobalt oxide NPs are reported by employing the USP synthesis route. Under USP process, an aqueous solution containing silica NPs and titanium complexes forms silica-titania nano-composite. A porous titania microsphere is obtained after etching of the silica-titania composite using HF. At initial stage of etching fetches a ball-in-ball structure consists of silica core covered with porous titania shell. Moreover, complete etching result in the vanishing of silica core and, finally, porous spherical shells of titania is obtained [209].

The formation of porous carbon under the USP technique has been reported. In this context, this technique is applied for the synthesis of several carbon nanostructures which occurs by alkali halocarboxylate decomposition (Fig. 12.11) [210].

As compared to tiresome multistep conventional approaches for porous carbon preparation, one step USP approach removes the issue of use of high cost template materials. Based on the variety of alkali halo-carboxylates such as lithium chloroacetate, sodium chloroacetate, potassium chloroacetate, lithium dichloroacetate, sodium dichloroacetate, and potassium dichloroacetate, a miscellaneous range of nanostructures has been synthesized via USP process [210].

12.6 Conclusions and Future Prospects

In summary, thermolysis (i.e., polyol, hydro/solvothermal, MW and sonochemical) approaches for the nanomaterial synthesis have been briefly described. Since precise control over shape, size, and dimension greatly alter the physiochemical properties. Therefore, the prepared nanomaterials encounter diverse area of interests into materials research community for the range of applications such as photoconductors, bio-imaging, laser materials, photocatalysis, biosensors, supercapacitors, etc. Polyol synthesis has unquestionably turned out to be a handy synthesis approach which assures the preparation of great quality nanomaterials. Ethylene glycol, diethylene glycol, glycerol, and butanediol are extensively applied as polyol solvents for the preparation of nanomaterials. Currently, a variety of nanomaterials such as elemental metals, metal oxides, and metal chalcogenides have been

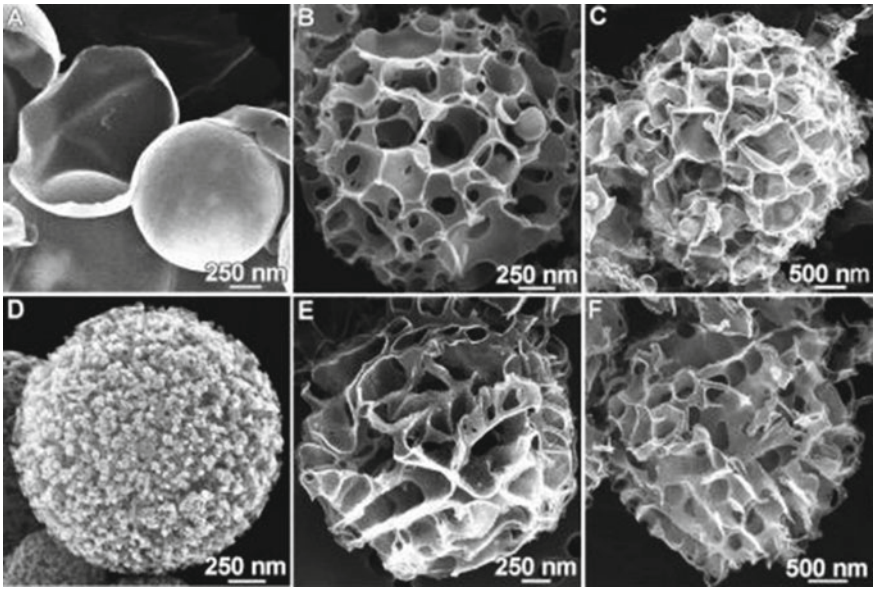

Fig. 12.11 SEM images of USP porous carbons. Reaction conditions: 1.5 M solutions, 700 °C, Ar at 1.0 slpm. Product from (A) lithium chloroacetate, (B) sodium chloroacetate, (C) potassium chloroacetate, (D) lithium dichloroacetate, (E) sodium dichloroacetate, and (F) potassium dichloroacetate. Reproduced with permission from ACS publisher [210]

synthesized via polyol mediated approach. Highly water dispersible and chelating properties of the polyols are extremely beneficial. During the synthesis, polyol act as solvent, reducing agent as well as capping agent which lead to surface functionalization as well as high colloidal stability of the NPs. Consequently, NPs with regular size distribution with less extent of agglomeration have been obtained. During the metal NPs synthesis in the polyol medium, the reductive character of the polyols is an added advantage which permits a straight reduction via heating of metal precursors. Also, higher boiling point of polyols fetches highly crystalline compounds during the synthesis. Due to these merits, polyol synthesis is broadly employed to attain materials with a range of applications as photocatalysis, MRI, sensing, photovoltaic, batteries, thin film, diluted transparent semiconductor, pigments, bio-imaging, and in drug delivery, etc. The polyol synthesis entails the preparation of heterostructured nanomaterials. Also, PEG exhibits control of the nucleation and growth of particles and particles coated with PEG show high bio-compatibility which permits the best possible cellular uptake of the pegylated NPs. However, there are also obvious restrictions to polyol synthesis. The fast thermal decomposition close to the boiling point of the polyols limits the availability of temperature choice of reactions.

The striking features of the MW-assisted synthesis exhibits rapid and uniform heating, fast reaction rate, higher yields, and shorter reaction time as compared to the usual heating techniques. Rapid synthesis of inorganic materials in aqueous phase under MW heating is observed. This unique approach leads to its cost effectiveness, energy saving, and a high product yield. Furthermore, the MW reactors with accurate power, temperature, and pressure controlled probes have been used for nanomaterials synthesis. However, detailed mechanism involved into MW synthesis and its consequence on reaction rate, nucleation, and growth in aqueous phase has been still matter of debate, and future research will be focussed in this direction. Precisely designed MW reactors will give an idea about the non-thermal heating issues involved under MW synthesis.

Hydrothermal and/or solvothermal routes are extensively utilized for the preparation of inorganic nanomaterials comprising metals, metal oxides, meal chalcogenides, and transition metals. These techniques are further extended for the synthesis of metal ions and linking organic ligands for metal organic framework (MOF)NPs.

The miscellaneous range of applications of ultrasound irradiation has been investigated in the synthesis of nanostructured materials. Sonochemical as well as ultrasonic spray pyrolysis techniques are used during the nanomaterials synthesis. Ultrasonic irradiation leads to acoustic cavitation. Bubbles are generated during cavitation, which can efficiently gather the ultrasound energy. After collapse of bubbles, massive amount of energy is released leading to localized hot spots with extremely high temperatures and pressures which are mainly responsible for chemical effects of ultrasound. By employing this route, elemental metals, metal alloys, metal oxides, metal sulfides, and metal carbides are synthesized. This synthesis approach is subsequently utilized for the synthesis of carbons, polymers and biomaterials, etc. During the synthesis of nano-composites, template-based strategy is used to obtain hollow structured materials via subsequent removal of template. Scale-up of materials and energy efficiency is the prime hindrance of sonochemical synthesis. Moreover, laboratory apparatus for sonochemical reactors is commercially available even though large scale apparatus remains quite rare. Future study will be to design precisely controlled sonochemical reactors for the large-scale production of the nanomaterials under ultrasonication.

In USP route, the ultrasound acts to nebulize the precursor solutions resulting production of micron-size droplets to facilitate the chemical reactions inside the reactor. The micro-reactors permit the simplistic control over elemental structure at the micron-size gauge. USP synthesis route is explored for the preparation of hetero-structure and/or composite materials. The synthesis of nanomaterials via USP generated nano-composites is vigorous as well as proficient. Moreover, processing of metal oxides via USP route is still inadequate mainly owing to the deficiency of appropriate precursors for metal oxides and uncontrolled fast sol-gel reactions. In view of the present restrictions, systematic development of new metal oxide precursors and precise control over the reaction parameters will be prime focus of the future study for the further advancement in USP technique.

Acknowledgements B.P.S. acknowledges the award through the Inspire Faculty (IFA17-MS-109) provided by DST, Government of India. Also, M.S. acknowledges the award through CSIR-SRA(9146-A) provided by CSIR, New Delhi, India.

References

1. Xia Y, Peidong Y, Sun Y, Wu Y, Mayers M, Gates B, Yin Y, Kim F, Yan H (2003) One dimensional nanostructures: synthesis, characterization, and applications. Adv Mater 15:353
2. Tsuji M (2017) Microwave-assisted synthesis of metallic nanomaterials in liquid phase. Chemistry 2:805
3. Jaiswal S, Smriti D (2017) Microwave-assisted eco-friendly synthesis and antimicrobial evaluation of Aryl-Triazole-1, 3, 4-Thiadiazols. J Med Res Innovat 1:17
4. Kumar VV, Kumar A (2020) Facile synthesis of flowerlike $LiFe_5O_8$ microspheres for electrochemical supercapacitors. Inorg Chem Commun 112:
5. Bharti A, Cheruvally G (2018) Surfactant assisted synthesis of Pt-Pd/MWCNT and evaluation as cathode catalyst for proton exchange membrane fuel cell. Int J Hydrogen Energy 31:14729
6. Soni AK, Joshi R, Singh BP, Kumar NN, Ningthoujam RS (2019) Near-infrared- and magnetic-field-responsive $NaYF_4:Er^{3+}/Yb^{3+}@SiO_2@AuNP@Fe_3O_4$ nanocomposites for hyperthermia applications induced by fluorescence resonance energy transfer and surface plasmon absorption. Appl ACS Nano Mater 2:7350
7. Dong H, Chen YC, Feldmann C (2015) Polyol synthesis of nanoparticles: status and options regarding metals, oxides, chalcogenides, and non-metal elements. Green Chem 17:4107
8. Baghbanzadeh M, Carbone L, Cozzoli PD, Kappe CO (2011) Microwave-assisted synthesis of colloidal inorganic nanocrystals. Angew Chem Int Ed 50:11312
9. Thorat ND, Shinde KP, Pawar SH, Barick KC, Betty CA, Ningthoujam RS (2012) Polyvinyl alcohol: an efficient fuel for synthesis of superparamagnetic LSMO nanoparticles for biomedical application. Dalton Trans 41:3060
10. Fiévet F, Vincent FF, Lagier JP, Dumont B, Figlarz M (1993) Controlled nucleation and growth of micrometre-size copper particles prepared by the polyol process. J Mater Chem 3:627
11. Wiley B, Herricks T, Sun Y, Xia Y (2004) Polyol synthesis of silver nanoparticles: use of chloride and oxygen to promote the formation of single-crystal, truncated cubes and tetrahedrons. Nano Lett 4:1733
12. El-Sayed MA (2001) Some interesting properties of metals confined in time and nanometer space of different shapes. Acc Chem Res 34:257
13. Song H, Kim F, Connor S, Somorjai GA, Yang P (2005) Pt nanocrystals: shape control and Langmuir-Blodgett monolayer formation. J Phys Chem, B 109:188
14. Xia X, Choi S, Herron JA, Lu N, Scaranto J, Peng HC, Wang J, Mavrikakis M, Kim MJ, Xia Y (2013) Facile synthesis of palladium right bipyramids and their use as seeds for overgrowth and as catalysts for formic acid oxidation. J Am Chem Soc 135:15706
15. Sun Y, Xia Y (2002) Shape-controlled synthesis of gold and silver nanoparticles. Science 298:2176
16. Toneguzzo P, Viau G, Acher O, Guillet F, Bruneton E, Fievet F (2000) CoNi and FeCoNi fine particles prepared by the polyol process: Physico-chemical characterization and dynamic magnetic properties J Mater Sci 35:3767
17. Jezequel D, Guenot J, Jouini N, Fievet F (1995) Suhinicrometer zinc oxide particles: Elaboration in pniyoi medium and morphological characteristics. J Mater Res 10:77
18. Liu C, Wu X, Klemmer T, Shukla N, Yang X, Weller D, Roy AG, Tanase M, Laughlin D (2004) Polyol process synthesis of monodispersed FePt nanoparticles. J Phys Chem B 108:6121

19. Watanabe K, Kura H, Sato T (2006) Transformation to L10 structure in FePd nanoparticles synthesized by modified polyol process. Sci Technol Adv Mater 7:145
20. Viau G, Fievet-Vincent F, Fievet F (1996) Nucleation and growth of bimetallic CoNi and FeNi monodisperse particles prepared in polyols. Solid State Ionics 84:259
21. Zhang B, Tu Z, Zhao F, Wang J (2013) Superparamagnetic iron oxide nanoparticles prepared by using an improved polyol method. Appl Surface Sci 266:375
22. Cai W, Wan J (2007) Facile synthesis of superparamagnetic magnetite nanoparticles in liquid polyols. J Colloid Interface Sci 305:366
23. Jézéquel D, Guenot J, Jouini N, Fiévet F (1995) Suhinicrometer zinc oxide particles: Elaboration in pniyoi medium and morphological characteristics. J Mater Res 10:77–83
24. Feldmann C, Jungk HO (2001) Polyol-mediated preparation of nanoscale oxide particles. Angew Chem Int Ed 40:359–362
25. Feldmann C (2003) Polyol-mediated synthesis of nanoscale functional materials. Adv Funct Mater 13:101
26. Ammar S, Helfen A, Jouini N, Fiévet F, Rosenman I, Villain F, Molinié P, Danot M (2001) Magnetic properties of ultrafine cobalt ferrite particles synthesized by hydrolysis in a polyol medium. J Mater Chem 11:186
27. Poul L, Jouini N, Fiévet F (2000) Layered hydroxide metal acetates (metal= zinc, cobalt, and nickel): elaboration via hydrolysis in polyol medium and comparative study. Chem Mater 12:3123
28. Prévot V, Forano C, Besse J (2005) Hydrolysis in polyol: new route for hybrid-layered double hydroxides preparation. Chem Mater 17:6695
29. Schmitt P, Brem N, Schunk S, Feldmann C (2011) Polyol-Mediated synthesis and properties of nanoscale molybdates/tungstates: color, luminescence, catalysis. Adv Funct Mater 21:3037
30. Parchur AK, Ningthoujam RS (2011) Preparation and structure refinement of Eu^{3+} doped CaMoO4 nanoparticles. Dalton Trans 40:7590
31. Maheshwary, Singh BP, Singh J, Singh RA (2014) Luminescence properties of Eu^{3+}-activated $SrWO_4$ nanophosphors-concentration and annealing effect. RSC Adv 4:32605
32. Maheshwary BP, Singh RA (2015) Color tuning in thermally stable Sm^{3+}-activated $CaWO_4$ nanophosphors. New J Chem 39:4494
33. Feldmann C, Roming M, Trampert K (2006) Polyol-Mediated Synthesis of Nanoscale CaF_2 and CaF_2:Ce,Tb. Small 2:1248
34. Parchur AK, Prasad AI, Rai SB, Tewari R, Sahu RK, Okram GS, Singh RA, Ningthoujam RS (2012) Observation of intermediate bands in Eu^{3+} doped YPO_4 host: Li^+ ion effect and blue to pink light emitter. AIP Adv 2:032119
35. Flores N, Franceschin G, Gaudisson T, Beaunier P, Yaacoub N, Grenèche JM, Valenzuela R, Ammar S (2018) Giant exchange-Bias in polyol-made $CoFe_2O_4$@CoO Core–shell like nanoparticles. Part Part Syst Charact 35:1800290
36. Tsuji M, Hikino S, Sano Y, Horigome M (2009) Preparation of Cu@Ag core–shell nanoparticles using a two-step polyol process under bubbling of N_2 gas. Chem Lett 38:518
37. Nguyen TT, Lau-Truong S, Mammeri F, Ammar S (2020) Star-shaped $Fe_{3-x}O_4$-Au core-shell nanoparticles: from synthesis to SERS application. Nanomaterials 10:294
38. Parchur AK, Ansari AA, Singh BP, Syed FN, Rai SB, Ningthoujam RS (2014) Enhanced luminescence of $CaMoO_4$:Eu by core@shell formation and its hyperthermia study after hybrid formation with Fe_3O_4: cytotoxicity assessment on human liver cancer cells and mesenchymal stem cells. Integer Biol 6:53
39. Mnasri W, Tahar LB, Beaunier P, Haidar DA, Boissière M, Sandre O, Ammar S (2020) Polyol-made luminescent and superparamagnetic β-$NaY_{0.8}Eu_{0.2}F_4$@γ-Fe_2O_3 core-satellites nanoparticles for dual magnetic resonance and optical imaging. Nanomaterials 10:393
40. Dong H, Kuzmanoski A, Gobi DM, Popescu R, Gerthsen D, Feldmann C (2014) Polyol-mediated C-dot formation showing efficient Tb^{3+}/Eu^{3+} emission. Chem Commun 50:7503–7506

41. Kumar A, Kuang Y, Liang Z, Sun X (2020) Microwave chemistry, recent advancements and eco-friendly microwave-assisted synthesis of nanoarchitectures and their applications: a review. Mater Today. NANO 11:
42. Zhu YJ, Chen F (2014) Microwave-assisted preparation of inorganic nanostructures in liquid phase. Chem Rev 114:6462
43. Collins MJ Jr (2010) Future trends in microwave synthesis. Med Chem 2:151
44. Nishioka M, Miyakawa M, Daino Y, Kataoka H, Koda H, Sato K, Suzuki TM (2013) Single-mode microwave reactor used for continuous flow reactions under elevated pressure. Ind Eng Chem Res 52:4683
45. Kappe CO (2004) Controlled microwave heating in modern organic synthesis. Angew Chem Int Ed 43:6250
46. Bilecka I, Niederberger M (2010) Microwave chemistry for inorganic nanomaterials synthesis. Nanoscale 2:1358
47. Robinson J, Kingman S, Irvine D, Licence P, Smith A, Dimitrakis G, Obermayer D, Kappe CO (2010) Understanding microwave heating effects in single mode type cavities-theory and experiment. Phys Chem Chem Phys 12:4750
48. Tsuji M, Hashimoto M, Nishizawa Y, Kubokawa M, Tsuji T (2005) Microwave-assisted synthesis of metallic nanostructures in solution. Chem Eur J 11:440
49. Baruwati B, Varma RS (2009) High value products from waste: grape pomace extract – a three-in-one package for the synthesis of metal nanoparticles. Chem Sus Chem 2:104
50. Hernandez CV, Mariscal MM, Esparza R, Yacaman MJ (2010) A synthesis route of gold nanoparticles without using a reducing agent. Appl Phys Lett 96:
51. Zhang ZW, Jia J, Ma YY, Weng J, Sun YA, Sun LP (2011) Microwave-assisted one-step rapid synthesis of folic acid modified gold nanoparticles for cancer cell targeting and detection. Med Chem Comm 2:1079
52. Hu B, Wang SB, Wang K, Zhang M, Yu SH (2008) Microwave-assisted rapid facile "green" synthesis of uniform silver nanoparticles: self-assembly into multilayered films and their optical properties. J Phys Chem C 112:11169
53. Luo YL (2007) A simple microwave-based route for size-controlled preparation of colloidal Pt nanoparticles. Mater Lett 2007:61
54. Mehta SK, Gupta SJ (2011) Time-efficient microwave synthesis of Pd nanoparticles and their electrocatalytic property in oxidation of formic acid and alcohols in alkaline media. Appl Electrochem 41:1407
55. Liu Y-Q, Zhang M, Wang F-X, Pan G-B (2012) Facile microwave-assisted synthesis of uniform single-crystal copper nanowires with excellent electrical conductivity. RSC Adv 2:11235
56. He Y, Zhong YL, Peng F, Wei XP, Su YY, Lu YM, Su S, Gu W, Liao LS, Lee S-T (2011) One-pot microwave synthesis of water-dispersible, ultraphoto- and pH-stable, and highly fluorescent silicon quantum dots. J Am Chem Soc 133:14192
57. Jing ZH, Zhan JH (2008) Fabrication and gas-sensing properties of porous ZnO nanoplates. Adv Mater 20:4547
58. Wu DS, Han CY, Wang SY, Wu NL, Rusakova IA (2002) Microwave-assisted solution synthesis of SnO nanocrystallites. Mater Lett 53:155
59. Wang HE, Xi LJ, Ma RG, Lu ZG, Chung CY, Bello I, Zapien JA (2012) Microwave-assisted hydrothermal synthesis of porous SnO_2 nanotubes and their lithium ion storage properties. J Solid State Chem 190:104
60. Zhang PL, Yin S, Sato T (2009) Synthesis of high-activity TiO_2 photocatalyst via environmentally friendly and novel microwave assisted hydrothermal process. Appl Catal B 89:118
61. Muraliganth T, Murugan AV, Manthiram A (2009) Facile synthesis of carbon-decorated single-crystalline Fe_3O_4 nanowires and their application as high performance anode in lithium ion batteries. Chem Commun 131:7360
62. Meher SK, Rao GR (2011) Effect of microwave on the nanowire morphology, optical, magnetic, and pseudocapacitance behavior of Co_3O_4. J Phys Chem C 115:25543

63. Zhu HT, Zhang CY, Tang YM, Wang JX (2007) Novel synthesis and thermal conductivity of CuO nanofluid. J Phys Chem C 111:1646
64. Ruong TT, Liu YZ, Ren Y, Trahey L, Sun YG (2012) Morphological and crystalline evolution of nanostructured MnO_2 and its application in lithium–air batteries. ACS Nano 6:8067
65. Bondioli F, Ferrari AM, Leonelli C, Siligardi C, Pellacani GC (2001) Microwave-hydrothermal synthesis of nanocrystalline zirconia powders. J Am Ceram Soc 84:2728
66. Hariharan V, Radhakrishnan S, Parthibavarman M, Dhilipkumar R, Sekar C (2011) Synthesis of polyethylene glycol (PEG) assisted tungsten oxide (WO_3) nanoparticles for l-dopa bio-sensing applications. Talanta 85:2166
67. Wei GD, Qin WP, Zhang DS, Wang GF, Kim RJ, Zheng KZ, Wang LL (2009) Synthesis and field emission of MoO_3 nanoflowers by a microwave hydrothermal route. J Alloys Compd 481:417
68. Liao XH, Zhu JM, Zhu JJ, Xu JZ, Chen HY (2001) Preparation of monodispersed nanocrystalline CeO_2 powders by microwave irradiation. Chem Commun 937
69. Zawadzki M (2008) Preparation and characterization of ceria nanoparticles by microwave-assisted solvothermal process. J Alloys Compd 451:297
70. de Moura AP, de Oliveira LH, Paris EC, Li MS, Andrés J, Varela JA, Longo E, Viana Rosa IL (2011) Photolumiscent properties of nanorods and nanoplates Y_2O_3: Eu_{3+}. J Fluoresc 21:1431
71. Joshi R, Singh BP, Ningthoujam RS (2020) Confirmation of highly stable 10 nm sized Fe_3O_4 nanoparticle formation at room temperature and understanding of heat generation under AC magnetic fields for potential application in hyperthermia. AIP Adv 10
72. Joshi R, Perala RS, Srivastava M, Singh BP, Ningthoujam RS (2019) Heat generation from magnetic fluids under alternating current magnetic field or induction coil for hyperthermia-based cancer therapy: basic principle. J Radiat Cancer Res 10:156
73. Hong RY, Pan TT, Li HZ (2006) Microwave synthesis of magnetic Fe_3O_4 nanoparticles used as a precursor of nanocomposites and ferrofluids. J Magn Magn Mater 303:60
74. Miao F, Hua W, Hu L, Huang KM (2011) Magnetic Fe_3O_4 nanoparticles prepared by a facile and green microwave-assisted approach Mater Lett 65:1031
75. Parsons JG, Luna C, Botez CE, Elizalde J, Torresdey JLG (2009) Microwave-assisted synthesis of iron(III) oxyhydroxides/oxides characterized using transmission electron microscopy, X-ray diffraction, and X-ray absorption spectroscopy. J Phys Chem Solids 70:555
76. Figueroa LA, Alvarez OM, Cruz JS, Contreras RG, Torres LSA, de la F. Hernández J, Arrocena MCA (2017) Nanomaterials made of non-toxic metallic sulfides: a systematic review of their potential biomedical applications. Mater Sci Eng C 76:1305
77. Tiwari A, Dhoble SJ (2016) Stabilization of ZnS nanoparticles by polymeric matrices: syntheses, optical properties and recent applications. RSC Adv 6:64400
78. Zhao Y, Liao XH, Hong JM, Zhu JJ (2004) Synthesis of lead sulfide nanocrystals via microwave and sonochemical methods. Mater Chem Phys 87:149
79. Mu CF, Yao QZ, Qu XF, Zhou GT, Li ML, Fu SQ (2010) Controlled synthesis of various hierarchical nanostructures of copper sulfide by a facile microwave irradiation method. Colloids Surf A 371:14
80. Zhu JJ, Zhou MG, Xu JZ, Liao XH (2001) Rapid synthesis of nanocrystalline SnO_2 powders by microwave heating method. Mater Lett 47:25
81. Zhao Y, Hong JM, Zhu JJ (2004) Microwave-assisted self-assembled ZnS nanoballs. J Cryst Growth 270:438
82. Xing RM, Liu SH, Tian SF (2011) Microwave-assisted hydrothermal synthesis of biocompatible silver sulfide nanoworms. J Nanopart Res 13:4847
83. Liao XH, Wang H, Zhu JJ, Chen HY (2001) Preparation of Bi_2S_3 nanorods by microwave irradiation. Mater Res Bull 36:2339

84. Shao MW, Kong LF, Li Q, Yu WC, Qian YT (2003) Microwave-assisted synthesis of tube-like HgS nanoparticles in aqueous solution under ambient condition. Inorg Chem Commun 6:737
85. Zhang WJ, Li DZ, Chen ZX, Sun M, Li WJ, Lin Q, Fu XZ (2011) Microwave hydrothermal synthesis of AgInS2 with visible light photocatalytic activity. Mater Res Bull 46:975
86. Zhang WJ, Li DZ, Sun M, Shao Y, Chen ZX, Xiao GC, Fu XZ (2010) Microwave hydrothermal synthesis and photocatalytic activity of AgIn5S8 for the degradation of dye. J Solid State Chem 183:2466
87. Bensebaa F, Durand C, Aouadou A, Scoles L, Du X, Wang D, Page YL (2010) A new green synthesis method of $CuInS_2$ and $CuInSe_2$ nanoparticles and their integration into thin films. J Nanopart Res 12:1897
88. Apte SK, Garaje SN, Bolade RD, Ambekar JD, Kulkarni MV, Naik SD, Gosavi SW, Baeg JO, Kale BB (2010) Hierarchical nanostructures of $CdIn_2S_4$ via hydrothermal and microwave methods: efficient solar-light-driven photocatalysts. J Mater Chem 20:6095
89. Li L, Qian HF, Ren JC (2005) Rapid synthesis of highly luminescent CdTe QDs in the aqueous phase by microwave irradiation with controllable temperature. Chem Commun 528
90. Zhu JJ, Palchik O, Chen SG, Gedanken A (2000) Microwave Assisted Preparation of CdSe, PbSe, and $Cu_{2-x}Se$ Nanoparticles J Phys Chem B 104:7344
91. Gawande MB, Goswami A, Asefa T, Guo H, Biradar AV, Peng DL, Zboril R, Varma RS (2015) Core–shell nanoparticles: synthesis and applications in catalysis and electrocatalysis. Chem Soc Rev 44:7540
92. Belousov OV, Belousova NV, Sirotina AV, Solovyov LA, Zhyzhaev AM, Zharkov SM, Mikhlin YL (2011) Formation of bimetallic Au-Pd and Au-Pt nanoparticles under hydrothermal conditions and microwave irradiation. Langmuir 27:11697
93. Yu JC, Hu XL, Li Q, Zheng Z, Xu YM (2006) Synthesis and characterization of core-shell selenium/carbon colloids and hollow carbon capsules. Chem Eur J 12:548
94. Zhang H, Yin YJ, Hu YJ, Li CY, Wu P, Wei SH, Cai CX (2010) Pd@Pt Core−shell nanostructures with controllable composition synthesized by a microwave method and their enhanced electrocatalytic activity toward oxygen reduction and methanol oxidation. J Phys Chem 114:11861
95. Bahadur NM, Watanabe S, Furusawa T, Sato M, Kurayama F, Siddiquey IA, Kobayashi Y, Suzuki N (2011) Rapid one-step synthesis, characterization and functionalization of Silica coated gold nanoparticles. Colloid Surface Physicochem Eng Aspects 392:137
96. Yu J, Yu X (2008) The greenhouse gas emissions and fossil energy requirement of bioplastics from cradle to gate of a biomass refinery. Environ Sci Technol 42:
97. Ming B, Li J, Kang F, Pang G, Zhang Y, Liang C, Xu J, Wang X (2012) Microwave–hydrothermal synthesis of birnessite-type MnO_2 nanospheres as supercapacitor electrode materials. J Power Sources 198:428
98. Frank C (2000) Hollow capsule processing through colloidal templating and self-assembly. Chem Eur J 6:413
99. An K, Hyeon T (2009) Synthesis and biomedical applications of hollow nanostructures. Nano Today 4:359
100. Li X, Sun P, Yang T, Zhao J, Wang Z, Wang W, Liu Y, Lu G, Du Y (2013) Template-free microwave-assisted synthesis of ZnO hollow microspheres and their application in gas sensing. Cryst Eng Comm 15:2949
101. Zou S, Xu X, Zhu Y, Cao C (2017) Microwave-assisted preparation of hollow porous carbon spheres and as anode of lithium-ion batteries. Microporous Mesoporous Mater 251:114
102. Li J, Chen Z, Wang RJ, Proserpio DM (1999) Low temperature route towards new materials: solvothermal synthesis of metal chalcogenides in ethylenediamine. Coord Chem Rev 192:707
103. Sue K, Suzuki M, Arai K, Ohashi T, Ura H, Matsui K, Hakuta Y, Hayashi H, Watanabe M, Hiaki T (2006) Size-controlled synthesis of metal oxide nanoparticles with a flow-through supercritical water method. Green Chem 8:634

104. Andelman T, Tan MC, Riman RE (2010) Thermochemical engineering of hydrothermal crystallisation processes. Mater Res Innov 14:9
105. Kashchiev D (1982) On the relation between nucleation work, nucleus size, and nucleation rate. J Chem Phys 76:5098
106. Uematsu M, Franck EU (1981) Static dielectric constant of water and steam. J Phys Chem Refer Data 9:1291
107. Li J, Wu Q, Wu J. Synthesis of nanoparticles via solvothermal and hydrothermal methods. Handbook of nanoparticles. https://doi.org/10.1007/978-3-319-13188-7_17-1
108. Li Y, Duan X, Liao H, Qian Y (1998) Self-regulation synthesis of nanocrystalline $ZnGa_2O_4$ by hydrothermal reaction. Chem Mater 10:17
109. Niederberger M, Pinna N, Polleux J, Antonietti M (2004) A general soft-chemistry route to perovskites and related materials: synthesis of $BaTiO_3$, $BaZrO_3$, and $LiNbO_3$. Nanoparticles Angew Chem Int Ed 43:2270
110. Srivastava BB, Kuang A, Mao Y (2015) Persistent luminescent sub-10 nm Cr doped $ZnGa_2O_4$ nanoparticles by a biphasic synthesis route. Chem Commun 51:7372
111. Jiang L, Yang M, Zhu S, Pang G, Feng S (2008) Phase evolution and morphology control of ZnS in a solvothermal system with a single precursor. J Phys Chem C 112:15281
112. Zhang Y, Li Y (2004) Synthesis and characterization of monodisperse doped ZnS nanospheres with enhanced thermal stability. J Phys Chem B 108:17805
113. Cozzoli PD, Manna L, Curri ML, Kudera S, Giannini C, Striccoli M, Agostiano A (2005) Shape and phase control of colloidal ZnSe nanocrystals. Chem Mater 17:1296
114. Li XH, Li JX, Li GD, Liu DP, Chen JS (2007) Controlled synthesis, growth mechanism, and properties of monodisperse CdS colloidal spheres. Chem A Eur J 13:8754
115. Ningthoujam RS, Gajbhiye NS (2015) Synthesis, electron transport properties of transition metal nitrides and applications. Prog Mater Sci 70:50
116. Xie Y, Qian Y, Wang W, Zhang S, Zhang Y (1996) A benzene-thermal synthetic route to nanocrystalline GaN. Science 272:1926
117. Purdy AP (1999) Ammonothermal synthesis of cubic gallium nitride. Chem Mater 11:1648
118. Mazumder B, Chirico P, Hector AL (2008) Direct solvothermal synthesis of early transition metal nitrides. Inorg Chem 47:9684
119. Hu B, Wang K, Wu L, Yu SH, Antonietti M, Titirici MM (2010) Engineering carbon materials from the hydrothermal carbonization process of biomass. Adv Mater 22:813
120. Titirici M-M, Antonietti M, Baccile N (2008) Hydrothermal carbon from biomass: a comparison of the local structure from poly-to monosaccharides and pentoses/hexoses. Green Chem 10:1204
121. Titirici MM, Thomas A, Antonietti M (2007) Replication and coating of silica templates by hydrothermal Carbonization. Adv Funct Mater 17:1010
122. Titirici M-M, Antonietti M (2010) Chemistry and materials options of sustainable carbon materials made by hydrothermal carbonization. Chem Soc Rev 39:103
123. Wang WZ, Huang JY, Ren ZF (2004) Synthesis of germanium nanocubes by a low-temperature inverse micelle solvothermal technique. Langmuir 21:751
124. Wang WZ, Poudel B, Huang JY, Wang DZ, Kunwar S, Ren ZF (2005) Synthesis of gram-scale germanium nanocrystals by a low-temperature inverse micelle solvothermal route. Nanotechnology 16:1126
125. Rowsell JLC, Yaghi OM (2005) Strategies for hydrogen storage in metal–organic frameworks. Angew Chem Int Ed 44:4670
126. Li J-R, Kuppler RJ, Zhou H-C (2009) Selective gas adsorption and separation in metal–organic frameworks. Chem Soc Rev 38:1477
127. Carpenter MK, Moylan TE, Kukreja RS, Atwan MH, Tessema MM (2012) Solvothermal synthesis of platinum alloy nanoparticles for oxygen reduction electrocatalysis. J Am Chem Soc 134:8535
128. Sadakiyo M, Yamada T, Kitagawa H (2009) Rational designs for highly proton-conductive metal−organic frameworks. J Am Chem Soc 131:9906

129. Lee J, Farha OK, Roberts J, Scheidt KA, Nguyen ST, Hupp JT (2009) Metal-organic framework materials as catalysts. Chem Soc Rev 38:1450
130. Rieter WJ, Taylor KM, An H, Lin W (2006) Nanoscale metal-organic frameworks as potential multimodal contrast enhancing agents. J Am Chem Soc 128:9024
131. McKinlay AC, Morris RE, Horcajada P, Férey G, Gref R, Couvreur P, Serre C (2010) BioMOFs: metal-organic frameworks for biological and medical applications. Angew Chem Int Ed 49:6260
132. Pashow KMLT, Rocca JD, Xie Z, Tran S, Lin W (2009) Postsynthetic modifications of iron-carboxylate nanoscale metal-organic frameworks for imaging and drug delivery. J Am Chem Soc 131:14261
133. Taylor KML, Jin A, Lin W (2008) Surfactant assisted synthesis of nanoscale gadolinium metal–organic frameworks for potential multimodal imaging. Angew Chem Int Ed 47:7722
134. Taylor KML, Rieter WJ, Lin W (2008) Manganese-based nanoscale metal-organic frameworks for magnetic resonance imaging. J Am Chem Soc 130:14358
135. Rieter WJ, Taylor KML, Lin W (2007) Surface modification and functionalization of nanoscale metal-organic frameworks for controlled release and luminescence sensing. J Am Chem Soc 129:9852
136. Suslick KS, Flannigan DJ (2008) Inside a collapsing bubble: sonoluminescence and the conditions during cavitation. Annu Rev Phys Chem 59:659
137. Suslick KS (1990) Sonochemistry. Science 247:1439
138. Suslick KS, Doktycz SJ (1990) Advances in sono-chemistry, vol 1. Mason TJ (ed), JAI Press, New York, pp 197
139. Frenzel H, Schultes H (1934) Luminescence in water carrying supersonic waves. Z Phys Chem 27b:421; Suslick KS (1995) MRS Bull 20:29
140. Bang JH, Suslick KS (2010) Applications of ultrasound to the synthesis of nanostructured materials. Adv Mater 22:1039
141. Dhas NA, Raj CP, Gedanken A (1998) Synthesis, characterization, and properties of metallic copper nanoparticles. Chem Mater 10:1446; Su CH, Wu PL, Yeh CS (2003) Sonochemical synthesis of well-dispersed gold nanoparticles at the ice temperature. J Phys Chem B 107:14240
142. Caruso RA, Kumar MA, Grieser F (2002) Sonochemical formation of gold sols. Langmuir 18:7831
143. Iglesias AS, Santos IP, Juste JP, González BR, García de Abajo FJ, Marzán LML (2006) Synthesis and optical properties of gold nanodecahedra with size control. Adv Mater 18:2529
144. Santos IP, Iglesias AS, García de Abajo FJ, Marzán LML (2007) Environmental optical sensitivity of gold nanodecahedra. Adv Funct Mater 17:1443
145. Jiang LP, Xu S, Zhu JM, Zhang JR, Zhu JJ, Chen HY (2004) Ultrasonic-assisted synthesis of monodisperse single-crystalline silver nanoplates and gold nanorings. Inorg Chem 43:5877
146. Fujimoto T, Terauchi S, Umehara H, Kojima I, Henderson W (2001) Sonochemical preparation of single-dispersion metal nanoparticles from metal salts. Chem Mater 13:1057
147. Nemamcha A, Rehspringer JL, Khatmi D (2006) Synthesis of palladium nanoparticles by sonochemical reduction of palladium (II) nitrate in aqueous solution. J Phys Chem B 110:383
148. Khalil H, Mahajan D, Rafailovich M, Gelfer M, Pandya K (2004) Synthesis of zerovalent nanophase metal particles stabilized with poly (ethylene glycol). Langmuir 20(16):6896
149. Wang H, Zhu JJ, Zhu JM, Chen HY (2002) Sonochemical method for the preparation of bismuth sulfide nanorods. J Phys Chem B 106:3848
150. Li HL, Zhu YC, Chen SG, Palchik O, Xiong J, Koltypin Y, Gofer Y, Gedanken A (2003) A novel ultrasound-assisted approach to the synthesis of CdSe and CdS nanoparticles. J Solid State Chem 172:102
151. Zhu JJ, Aruna ST, Koltypin Y, Gedanken A (2000) A novel method for the preparation of lead selenide: pulse sonoelectrochemical synthesis of lead selenide nanoparticles. Chem Mater 12:143

152. Wang WZ, Geng Y, Yan P, Liu FY, Xie Y, Qian YT (1999) A novel mild route to nanocrystalline selenides at room temperature. J Am Chem Soc 121:4062
153. Zhu JJ, Xu S, Wang H, Zhu JM, Chen HY (2003) Sonochemical synthesis of CdSe hollow spherical assemblies via an In-Situ template route. Adv Mater 15:156
154. Li H, Zhu Y, Chen S, Palchik O, Xiong J, Koltypin Y, Gofer Y, Gedanken A (2003) A novel ultrasound-assisted approach to the synthesis of CdSe and CdS nanoparticles. J Solid State Chem 172:102
155. Wang H, Xu S, Zhao X-N, Zhu J-J, Xin X-Q (2002) Sonochemical synthesis of size-controlled mercury selenide nanoparticles. Mater Sci Eng, B 96:60
156. Mdleleni MM, Hyeon T, Suslick KS (1998) Sonochemical synthesis of nanostructured molybdenum sulfide. J Am Chem Soc 120:6189
157. Xie Y, Zheng X, Jiang X, Lu J, Zhu L (2002) Sonochemical Synthesis and Mechanistic Study of Copper Selenides $Cu_{2-x}Se$, β-CuSe, and Cu_3Se_2 Inorg Chem 41:387
158. Li B, Xie Y, Huang J, Liu Y, Qian Y (2000) Sonochemical synthesis of nanocrystalline copper tellurides Cu_7Te_4 and Cu_4Te_3 at room temperature. Chem Mater 12:2614
159. Pejova B, Grozdanov I, Nesheva D, Petrova A (2008) Size-dependent properties of sonochemically synthesized three-dimensional arrays of close-packed semiconducting $AgBiS_2$ Quantum Dots. Chem Mater 20:2551
160. Okitsu K, Nagata Y, Mizukoshi Y, Maeda Y, Bandow H, Yamamoto TA (1997) Synthesis of palladium nanoparticles with interstitial carbon by sonochemical reduction of tetrachloropalladate (II) in aqueous solution. J Phys Chem B 101:5470
161. Nikitenko S, Koltypin Y, Palchik O, Felner I, Xu XN, Gedanken A (2001) Synthesis of highly magnetic, air stable iron-iron carbide nanocrystalline particles by using power ultrasound. Angew Chem Intd Ed 40:4447
162. Hyeon T, Fang M, Suslick KS (1996) Nanostructured molybdenum carbide: sonochemical synthesis and catalytic properties. J Am Chem Soc 118:5492–5493
163. Suslick KS, Hyeon T, Fang M, Ries JT, Cichowlas AA (1996) Sonochemical synthesis of nanophase metals, alloys and carbides. Mater Sci Forum 225–227:903–912
164. Bellissent R, Galli G, Hyeon T, Migliardo P, Parette P, Suslick KS, Noncryst J (1996) Magnetic and structural properties of amorphous transition metals and alloys. Solids 205:656
165. Mizukoshi Y, Okitsu K, Maeda Y, Yamamoto TA, Oshima R, Nagata Y (1997) Sonochemical preparation of bimetallic nanoparticles of gold/palladium in aqueous solution. J Phys Chem B 101:7033
166. Egami T (1984) Magnetic amorphous alloys: physics and technological applications. Rep Prog Phys 47:1601
167. Shafi K, Gedanken A, Prozorov R (1998) Sonochemical preparation and characterization of nanosized amorphous Co–Ni alloy powders. J Mater Chem 8:769
168. Li Q, Li H, Pol VG, Bruckental I, Koltypin Y, Moreno JC, Nowik I, Gedanken A (2003) Sonochemical synthesis, structural and magnetic properties of air-stable Fe/Co alloy nanoparticles. New J Chem 27:1194
169. Vinodgopal K, He Y, Ashokkumar M, Grieser F (2006) Sonochemically prepared platinum-ruthenium bimetallic nanoparticles. J Phys Chem B 110:3849
170. Srivastava DN, Chappel S, Palchik O, Zaban A, Gedanken A (2002) Sonochemical synthesis of mesoporous tin oxide. Langmuir 18:4160
171. Wang Y, Yin L, Gedanken A (2002) Sonochemical synthesis of mesoporous transition metal and rare earth oxides. Ultrason Sonochem 9:285
172. Bhatte K, Fujita S, Arai M, Pandit A, Bhanage B (2011) Ultrasound assisted additive free synthesis of nanocrystalline zinc oxide. Ultrason Sonochem 18:54
173. Jung S-H, Oh E, Lee K-H, Yang Y, Park CG, Park W, Jeong S-H (2008) Sonochemical preparation of shape-selective ZnO nanostructures. Cryst Growth Des 8:265–269
174. Yu JC, Yu J, Ho W, Zhang L (2001) Preparation of highly photocatalytic active nano-sized TiO_2 particles via ultrasonic irradiation. Chem Commun:1942
175. Zhang D, Fu H, Shi L, Pan C, Li Q, Chu Y, Yu W (2007) Synthesis of CeO_2 Nanorods via Ultrasonication Assisted by Polyethylene Glycol. Inorg Chem 46:2446

176. Krishnan CVC, Burger J, Chu C (2006) Polymer-assisted growth of molybdenum oxide whiskers via a sonochemical process. J Phys Chem B 110:20182
177. Mao C-J, Pan H-C, Wu X-C, Zhu J-J, Chen H-Y (2006) Sonochemical route for self-assembled V_2O_5 bundles with spindle-like morphology and their novel application in serum albumin sensing. J Phys Chem B 110:14709
178. Dutta DP, Sudarsan V, Srinivasu P, Vinu A, Tyagi AK (2008) Indium oxide and europium/dysprosium doped indium oxide nanoparticles: sonochemical synthesis, characterization, and photoluminescence studies. J Phys Chem C 112:6781
179. Geng J, Zhu JJ, Lu DJ, Chen HY (2006) Hollow $PbWO_4$ Nanospindles via a Facile Sonochemical Route. Inorg Chem 45:8403
180. Geng J, Hou WH, Lv YN, Zhu JJ, Chen HY (2005) One-Dimensional $BiPO_4$ nanorods and two-dimensional BiOCl lamellae:fast low temperature sonochemical synthesis, characterization, and growth mechanism. Inorg Chem 44:8503
181. Dutta DP, Ghildiyal R, Tyagi AK (2009) Luminescent properties of doped zinc aluminate and zinc gallate white light emitting nanophosphors prepared via sonochemical method. J Phys Chem C 113:16954
182. Dhas NA, Suslick KS (2005) Sonochemical preparation of hollow nanospheres and hollow nanocrystals. J Am Chem Soc 127:2368
183. Bang JH, Suslick KS (2007) Sonochemical synthesis of nanosized hollow hematite. J Am Chem Soc 129:2242
184. Du N, Zhang H, Chen BD, Yu JB, Ma XY, Liu ZH, Liu ZH, Zhang YQ, Yang DR, Huang XH, Tu JP (2007) Porous Co_3O_4 nanotubes derived from $Co_4(CO)_{12}$ clusters on carbon nanotube templates: a highly efficient material for Li-battery applications. Adv Mater 19:4505
185. Wang J, Loh KP, Zhong YL, Lin M, Ding J, Foo YL (2007) Bifunctional FePt core-shell and hollow spheres: sonochemical preparation and self-assembly. Chem Mater 19:2566
186. Yin J, Qian X, Yin J, Shi M, Zhou G (2003) Preparation of ZnS/PS microspheres and ZnS hollow shells. Mater Lett 57:3859
187. Hernandez Y, Nicolosi V, Lotya M, Blighe FM, Sun Z, De S, McGovern IT, Holland B, Byrne M, Gun'Ko YK, Boland JJ, Niraj P, Duesberg G, Krishnamurthy S, Goodhue R, Hutchison J, Scardaci V, Ferrari VAC, Coleman JN (2008) High-yield production of graphene by liquid-phase exfoliation of graphite. Nat Nanotechnol 3:563
188. Coleman JN, Lotya M, O'Neill A, Bergin SD, King PJ, Khan U, Young K, Gaucher A, De S, Smith RJ, Shvets IV, Arora SK, Stanton G, Kim HY, Lee K, Kim GT, Duesberg GS, Hallam T, Boland JJ, Wang JJ, Donegan JF, Grunlan JC, Moriarty G, Shmeliov A, Nicholls RJ, Perkins JM, Grieveson EM, Theuwissen K, McComb DW, Nellist PD, Nicolosi V (2011) Two-dimensional nanosheets produced by liquid exfoliation of layered materials. Science 331:568
189. Toublan FJJ, Boppart S, Suslick KS (2006) Tumor targeting by surface-modified protein microspheres. J Am Chem Soc 128:3472
190. Suslick KS, Grinstaff MW (1990) Protein micro-encapsulation of non-aqueous liquids. J Am Chem Soc 112:7807
191. Grinstaff MW, Suslick KS (1991) Air-filled protein aceous microbubbles: synthesis of an echo-contrast agent. Proc Natl Acad Sci USA 88:7708
192. Xu H, Zeiger BW, Suslick KS (2013) Sonochemical synthesis of nanomaterials. Chem Soc Rev 42:2555
193. Kitano M, Kitano T, Hamabe S, Maeda T, Okabe J (1990) Growth of large tetrapod-like ZnO crystals: experimental considerations on kinetics of growth. Crys Growth 102:965
194. Gao T, Li Q, Wang T (2005) Sonochemical synthesis, optical properties, and electrical properties of core/shell-type ZnO nanorod/CdS nanoparticle composites. Chem Mater 17 (4):887
195. Morel AL, Nikitenko SI, Gionnet K, Wattiaux A, Him JLK, Labrugere C, Chevalier B, Deleris G, Petibois C, Brisson A, Simonoff M (2008) Sonochemical approach to the

synthesis of Fe_3O_4@SiO_2 core−shell nanoparticles with tunable properties. ACS Nano 2 (5):847
196. Gao T, Wang T (2004) Sonochemical synthesis of SnO_2 nanobelt/CdS nanoparticle core/shell heterostructures. Chem Commun 22:2558
197. Anandan S, Grieser F, Kumar MA (2008) Sonochemical synthesis of Au-Ag core-shell bimetallic nanoparticles. J Phys Chem C 112(39):15102
198. Salkar RA, Jeevanandam P, Aruna ST, Koltypin Y, GedankenJ A (1999) The sonochemical preparation of amorphous silver nanoparticles. Mater Chem 9:1333
199. Ranasinghe JC, Dikkumbura AS, Hamal P, Chen M, Khoury RA, Smith HT, Lopata K, Haber LH (2019) Monitoring the growth dynamics of colloidal gold-silver core-shell nanoparticles using in-situ second harmonic generation and extinction spectroscopy. J Chem Phys 151:
200. Kodas TT, Hampden-Smith M (1999) Aerosol processing of materials. Wiley-VCH, New York
201. Suh WH, Suslick KS (2005) Magnetic and porous nanospheres from ultrasonic spray pyrolysis. J Am Chem Soc 127:12007
202. Pluym TC, Powell QH, Gurav AS, Ward TL, Kodas TT, Wang LM, Glicksman HD (1993) Solid silver particle production by spray pyrolysis. J Aerosol Sci 24:383
203. Majumdar D, Kodas TT, Glicksman HD (1996) Gold particle generation by spray pyrolysis. Adv Mater 8:1020
204. Kim JH, Germer TA, Mulholland GW, Ehrman SH (2002) Size-monodisperse metal nanoparticles via hydrogen-free spray pyrolysis. Adv Mater 14:518
205. Nagashima K, Wada M, Kato A (1990) Preparation of fine Ni particles by the spray-pyrolysis technique and their film forming properties in the thick film method. J Mater Res 5:2828
206. Pluym TC, Kodas TT, Wang L-M, Glicksman HD (1995) Silver-palladium alloy particle production by spray pyrolysis. J Mater Res 10:1661
207. Vivekchand SRC, Gundiah G, Govindaraj A, Rao CNR (2004) A new method for the preparation of metal nanowires by the nebulized spray pyrolysis of precursors. Adv Mater 2004(16):153
208. Skrabalak SE, Suslick KS (2005) Porous MoS_2 synthesized by ultrasonic spray pyrolysis. J Am Chem Soc 127:9990
209. Suh WH, Jang AR, Suh Y-H, Suslick KS (2006) Porous, hollow, and ball-in-ball metal oxide microspheres: preparation, endocytosis, and cytotoxicity. Adv Mater 2006:18
210. Skrabalak SE, Suslick KS (2006) Porous carbon powders prepared by ultrasonic spray pyrolysis. J Am Chem Soc 128:12642